

Effects of CO₂, continental distribution, topography and vegetation changes on the climate at the Middle Miocene: a model study

A.-J. Henrot¹, L. François², E. Favre², M. Butzin³, M. Ouberdous², and G. Munhoven¹

¹Laboratory of Atmospheric and Planetary Physics, University of Liège, Liège, Belgium

²Unité de Modélisation du Climat et des Cycles Biogéochimiques, University of Liège, Liège, Belgium

³MARUM – Center for Marine Environmental Sciences, University of Bremen, Bremen, Germany

Received: 16 March 2010 – Published in Clim. Past Discuss.: 14 April 2010

Revised: 27 September 2010 – Accepted: 18 October 2010 – Published: 21 October 2010

Abstract. The Middle Miocene was one of the last warm periods of the Neogene, culminating with the Middle Miocene Climatic Optimum (MMCO, approximately 17–15 Ma). Several proxy-based reconstructions support warmer and more humid climate during the MMCO. The mechanisms responsible for the warmer climate at the MMCO and particularly the role of the atmospheric carbon dioxide are still highly debated. Here we carried out a series of sensitivity experiments with the model of intermediate complexity Planet Simulator, investigating the contributions of the absence of ice on the continents, the opening of the Central American and Eastern Tethys Seaways, the lowering of the topography on land, the effect of various atmospheric CO₂ concentrations and the vegetation feedback.

Our results show that a higher than present-day CO₂ concentration is necessary to generate a warmer climate at all latitudes at the Middle Miocene, in agreement with the terrestrial proxy reconstructions which suggest high atmospheric CO₂ concentrations at the MMCO. Nevertheless, the changes in sea-surface conditions, the lowering of the topography on land and the vegetation feedback also produce significant local warming that may, locally, even be stronger than the CO₂ induced temperature increases. The lowering of the topography leads to a more zonal atmospheric circulation and allows the westerly flow to continue over the lowered Plateaus at mid-latitudes. The reduced height of the Tibetan Plateau notably prevents the development of a monsoon-like circulation, whereas the reduction of elevations of the North American and European reliefs strongly increases precipitation from northwestern to eastern Europe.

The changes in vegetation cover contribute to maintain and even to intensify the warm and humid conditions produced by the other factors, suggesting that the vegetation-climate interactions could help to improve the model-data comparison.

1 Introduction

In a long-term climatic cooling trend, the Middle Miocene represents one of the last warm periods of the Neogene, culminating with the Middle Miocene Climatic Optimum, MMCO, that occurred at approximately 17–15 Ma (Zachos et al., 2001). Various proxy data support a warmer and more humid climate during the MMCO (Zachos et al., 2001; Mosbrugger et al., 2005; Bruch et al., 2007). Proxy-based studies suggest a warming at mid-latitudes of about +6 °C (Flower and Kennett, 1994) and a weak equator-to-pole latitudinal temperature gradient (Bruch et al., 2007). However, the climate mechanisms responsible for the warmer climate at the MMCO and, in particular, the role of the atmospheric carbon dioxide, CO₂, are still highly debated. Frequently, elevated greenhouse gas concentrations are cited as primary contributors to past warm climates (Shellito et al., 2003). However, estimates for the concentration of CO₂ in the atmosphere at the MMCO range from levels that are typical for Pleistocene glaciations to nearly twice the modern value. Pagani et al. (1999) calculated CO₂ levels of 180 to 290 ppmv from marine δ¹³C biological isotopic fractionation. Marine pH reconstructions from δ¹¹B also point towards a low CO₂ level between 140 and 300 ppmv (Pearson and Palmer, 2000), supporting a decoupling between CO₂ and temperature during the Middle Miocene. However,



Correspondence to: A.-J. Henrot
(alexandra.henrot@ulg.ac.be)

the reconstructions of Kürschner et al. (2008) based on leaf stomatal indices indicate much higher MMCO CO₂ levels between 300 and 600 ppmv. Reconstructions based on paleosoil analysis indicate an even higher CO₂ concentration of 850 ppmv (Retallack, 2009). However, CO₂ concentrations reconstructed on the basis of planktonic foraminiferal $\delta^{18}\text{O}$ temperature reconstructions are possibly biased due to estimates of ice volume or diagenesis (Pagani et al., 2010, Supplement). Alkenone-based temperature reconstructions could possibly lead to higher CO₂ concentration estimates for the Miocene (Pagani et al., 2010, Supplement).

The reconfiguration of inter-oceanic passages which significantly influences the ocean circulation may also have contributed to the MMCO climate (Bice et al., 2000; Von der Heydt and Dijkstra, 2008). The Central American Seaway and Eastern Tethys Seaway were notably open during the Middle Miocene (Herold et al., 2008), leading to significantly different ocean circulation patterns (Von der Heydt and Dijkstra, 2006).

Geological processes such as mountain uplift may also affect the atmospheric circulation and precipitation patterns (Gregory-Wodzicki, 2000; Harris, 2006). Although the positions of the continents were close to modern, most of the higher orogens got elevated during the Miocene, such as the Himalayas and the Tibetan Plateau (Currie et al., 2005; Harris, 2006), the Central Andes (Gregory-Wodzicki, 2000) as well as the Alps (Kuhleemann et al., 2006). Topography was therefore generally lower at the Middle Miocene than at present-day (Herold et al., 2008).

Finally it should also be noticed that the warm climate prevailing during the Middle Miocene led to vegetation changes. Broadleaved evergreen forests appear to have extended as far north as 45° N in North America and 52° N in Europe (Utescher et al., 2000). Such a change in the vegetation cover may have led to significant impacts on climate (Dutton and Barron, 1997).

Up to now, only a few climate model simulations have been performed for the Middle Miocene. Von der Heydt and Dijkstra (2006) used an AOGCM (Community Climate System Model (CCSM v.1.4)) to study the effect of ocean gateways on global ocean circulation patterns in the Late Oligocene to Early Miocene. Their results indicated that the different configuration of the ocean gateways may have significantly affected the global thermohaline circulation in the Miocene. However, they did not assess any topographic nor vegetation effect. They prescribed a flat land with a constant elevation of 350 m and a zonally constant vegetation distribution. The ocean model that they used furthermore had a flat bottom ocean at 5000 m depth. More recent climate modelling sensitivity experiments have particularly focused on the sensitivity of the Miocene climate to various atmospheric CO₂ concentrations using atmospheric models (Tong et al., 2009; You et al., 2009). Tong et al. (2009) used the NCAR Community Atmosphere Model (CAM v.3.1) and Community Land Model (CLM v.3.0) coupled to a slab ocean to

examine the sensitivity of the Middle Miocene climate to successive quasi-doubling of atmospheric CO₂ concentration (180 355 and 700 ppmv). You et al. (2009) used the same NCAR models coupled to a slab model to analyse the sensitivity of the MMCO climate to varying ocean heat fluxes derived from palaeo sea surface temperatures and successive quasi-doubling of atmospheric CO₂ concentrations (180 355 and 700 ppmv) and compared their global temperature estimations to available proxy data. Both studies required higher than present-day CO₂ concentrations to produce a warmer climate at the MMCO. However, Tong et al. (2009) and You et al. (2009) also found that the sole increase of CO₂ is not sufficient to produce the MMCO warming inferred from proxy-data. Finally, Herold et al. (2009) tested the impact of altered Andean and Tibetan Plateau elevations on the MMCO climate again with the same NCAR models, and fixed sea surface temperatures. Herold et al. (2009) indicated that the reduction of the Tibetan Plateau and Andes elevations significantly affects local temperatures. However, they also concluded that topography alone could not be a significant factor in reconciling the warm MMCO climate and the CO₂ concentration estimates.

The objective of the present study is to examine the contribution of several boundary condition changes to the warm MMCO climate and particularly to discuss the contribution of the vegetation feedback as a potential alternative mechanism to the large increase of CO₂ required by the models to produce a warmer climate at the MMCO. Therefore, we performed a series of simulation experiments with the Planet Simulator, where we have assessed the effects of the absence of ice on the continents, the opening of the Central American and Eastern Tethys Seaways, the lowering of the topography on land and the effect of various atmospheric CO₂ concentrations. We reconstructed the vegetation distribution for the Middle Miocene in response to the MMCO boundary conditions previously cited, using the CARAIB dynamic vegetation model. We then forced the Planet Simulator with the reconstructed Middle Miocene vegetation distribution to assess the vegetation feedback in response to the Middle Miocene simulated climate. We first describe our model setup (Sect. 2.1) and examine the response of surface climate (temperature, precipitation and low level winds) to the different forcings (Sect. 3). Finally, we discuss the contribution of the factors on the Middle Miocene climate, focusing in particular on the contribution of vegetation cover changes (Sect. 4).

2 Model and experimental design

The Planet Simulator (Fraedrich et al., 2005a,b) is an Earth system Model of Intermediate Complexity (EMIC). It has been used for present-day climate modelling studies (Fraedrich et al., 2005b; Grosfeld et al., 2007; Junge et al., 2005) as well as for various paleoclimatic studies focusing on

different past periods (Romanova et al., 2006; Henrot et al., 2009), notably the late Miocene (Micheels et al., 2009b). The model has proven usefulness in the comparison to proxy data (Henrot et al., 2009; Micheels et al., 2009a). The Planet Simulator present-day climate compares fairly well to ERA-40 reanalysis although it is affected by two major climatological biases: (1) a cold bias at high latitudes in winter of the hemisphere and (2) a global overestimation of the surface evaporation (Haberhorn et al., 2009). The central component of the Planet Simulator is PUMA-2, a spectral GCM with triangular truncation, based upon the Portable University Model of the Atmosphere, PUMA (Fraedrich et al., 1998). PUMA-2 solves the moist primitive equations, representing the conservation of momentum, mass and energy, on σ coordinates in the vertical. It also includes boundary layer, precipitation, interactive clouds and radiation parametrizations. For the present study, we configured it to use a T42 truncation and ten vertical equally spaced σ levels. The model atmosphere is coupled to a 50 m deep mixed-layer ocean, a thermodynamic sea-ice and a land surface and soil model.

Sea surface temperatures are computed from the net atmospheric heat flux at the surface. The transport of heat by oceanic surface currents is represented by an additional distribution of heat sources and sinks that is prescribed within the mixed-layer and the sea-ice and that varies monthly and spatially. Their distributions for the preindustrial period and the Middle Miocene were determined from preindustrial and Miocene experiments respectively, where sea surface temperature and sea-ice distributions were obtained from simulations with an updated version of the Hamburg LSG circulation model (developed by Maier-Reimer et al., 1993) (Butzin et al., 2010). This procedure allows the model to respond with a larger sensitivity to boundary condition changes than with prescribed sea-surface temperatures.

The land surface and soil models calculate the surface temperatures from a linearized energy balance equation and predict soil moisture on the basis of a simple bucket model. The influence of vegetation is represented by background albedo, roughness length and rooting depth. Their annual distributions are prescribed, and albedo may only change in grid-cells where snow is present. The distributions of surface albedo, roughness length and rooting depth were obtained from a preindustrial run and a Middle Miocene run of the dynamic vegetation model CARAIB (CARbon Assimilation In the Biosphere) (Otto et al., 2002; François et al., 2006; Laurent et al., 2008). CARAIB calculates the carbon fluxes between the atmosphere and the terrestrial biosphere and deduces the evolution of carbon pools, together with the relative abundances of a series of plant functional types. Its different modules respectively focus on the hydrological cycle, photosynthesis and stomatal regulation, carbon allocation and biomass growth, heterotrophic respiration and litter and soil carbon, and the distribution of the model plant types, as a function of productivity. Here we use a classification including 15 Plant Functional Types (PFTs), described

Table 1. Description of the simulation experiments. *P* refers to preindustrial conditions and *M* refers to Miocene conditions. Each one of the five columns corresponds to each of the five modified boundary conditions: ocean heat transfer, ice-sheet cover, atmospheric CO₂ concentration (in ppmv), topography and vegetation cover

Simulation	Ocean	Ice	CO ₂	Topo	Veg
CTRL	<i>P</i>	<i>P</i>	280	<i>P</i>	<i>P</i>
MM1	<i>M</i>	<i>M</i>	280	<i>P</i>	<i>P</i>
MM2	<i>M</i>	<i>M</i>	280	<i>M</i>	<i>P</i>
MM3	<i>M</i>	<i>M</i>	200	<i>M</i>	<i>P</i>
MM4	<i>M</i>	<i>M</i>	500	<i>M</i>	<i>P</i>
MM4-veg	<i>M</i>	<i>M</i>	500	<i>M</i>	<i>M</i>

in Utescher et al. (2007) and Galy et al. (2008). Model derived PFT assemblages can be translated into biomes to produce vegetation maps. The inputs of the model are meteorological variables, taken from meteorological databases or GCM simulation experiments.

2.1 Experimental setup

In this work we examine the potential contribution of several boundary condition forcings to the MMCO. We therefore perform a series of five sensitivity experiments where we have assessed the effects of the absence of ice on the continents, the opening of the Central American and Eastern Tethys Seaways, the lowering of the topography on land, of various atmospheric CO₂ concentrations and the effect of vegetation cover changes on climate (through surface albedo, roughness length and rooting depth, i. e., bucket size) in response to the Middle Miocene simulated climate. Table 1 lists the boundary condition changes applied for the series of experiments. The control experiment (CTRL) does not consider any of the changes and corresponds to a preindustrial state. All experiments have been run for 50 years and the results shown in Sect. 3 are means over the last 20 years of simulation, allowing 30 years for the model to equilibrate.

2.1.1 Land ice

According to Flower and Kennett (1994) who place the major growth of the East Antarctic Ice-Sheet around 14.8 to 12.9 Ma (i. e. later than the MMCO), and Pekar and DeConto (2006) who suggest that only a reduced East Antarctic Ice-Sheet was present during the Middle Miocene (17 to 16 Ma), we removed ice-sheets from Antarctica and Greenland in the whole series of Miocene experiments. This mainly affects the surface albedo on land. In the absence of ice-sheets in Greenland and Antarctica the surface albedo is set equal to the bare soil value (20%). The continental land-ice cover for the (preindustrial) control experiment has been derived from Peltier's ICE-5G (Peltier, 2004), considering that grid-cells covered by an ice fraction greater than 50% are completely covered by ice.

2.1.2 Ocean and sea-ice

There is currently no global proxy-based SST reconstruction available for the MMCO that could be directly used with GCMs. Furthermore several biases towards notably colder temperatures have been detected in the oxygen isotope palaeo SST estimates (Pearson et al., 2007). Williams et al. (2005) also suggested that the Miocene tropical sea surface temperatures may be underestimated in the current reconstructions, due notably to diagenesis. We therefore preferred to use as initial conditions over ocean grid points sea-surface temperature and sea-ice distributions derived from simulations of the updated Hamburg LSG circulation model, which includes a simple atmospheric energy balance model permitting that the LSG SSTs freely adjust to ocean circulation changes (Butzin et al., 2010). Butzin et al. (2010) performed several simulation experiments to assess the sensitivity of benthic carbon isotope records to various seaway configurations and sea-ice scenarios. In this work, we use as initial oceanic conditions for all the Miocene simulation experiments the sea-surface temperature and sea-ice distributions from one LSG simulation featuring open Central American and Eastern Tethys Seaways, a filled Hudson Bay and a closed Bering Strait, according to Gladenkov et al. (2002), a fixed atmospheric CO₂ concentration of 282 ppmv, and sea ice extent around 90% of the present-day value. Preindustrial LSG results were also used to derive the preindustrial sea-surface temperature and sea-ice distributions for the control run of our series. The LSG Miocene run's spinup is 10 000 years long and the LSG sea-surface temperatures and sea-ice cover used here as initial conditions are means over the last 50 years of simulation. The LSG sea-surface temperature and sea-ice cover for the preindustrial and the Miocene are shown in Fig. 1. In the Miocene LSG simulation, the opening of the Central American Seaway freshened the upper part of North Atlantic while salinities increased in the other oceans. The Meridional Overturning Circulation (MOC) in the Atlantic Ocean weakened. As a consequence, the upper North Atlantic got cooler and the South Atlantic warmer. The Eastern Tethys Seaway weakly impacted on Indian Ocean heat transport (Butzin et al., 2010). The impact of a closed Bering Strait is more convoluted (the Bering Strait first opened in the Late Miocene at about 5.4–5.3 Ma, Gladenkov et al., 2002). A closed Bering Strait may reinforce the impact of the open Central American Seaway. An open Bering Strait in a Late Miocene LSG sensitivity experiment mitigated the effect of the open Central American Seaway, because of a freshwater export from the Arctic Ocean into the North Pacific via the Bering Strait (unpublished results). The water flux through the open Bering Strait in the Miocene LSG experiment is opposite to the present-day water flux from the North Pacific to the Arctic Ocean, which is in line with results of fully coupled freshwater perturbation experiments under present-day conditions (Okumura et al., 2009).

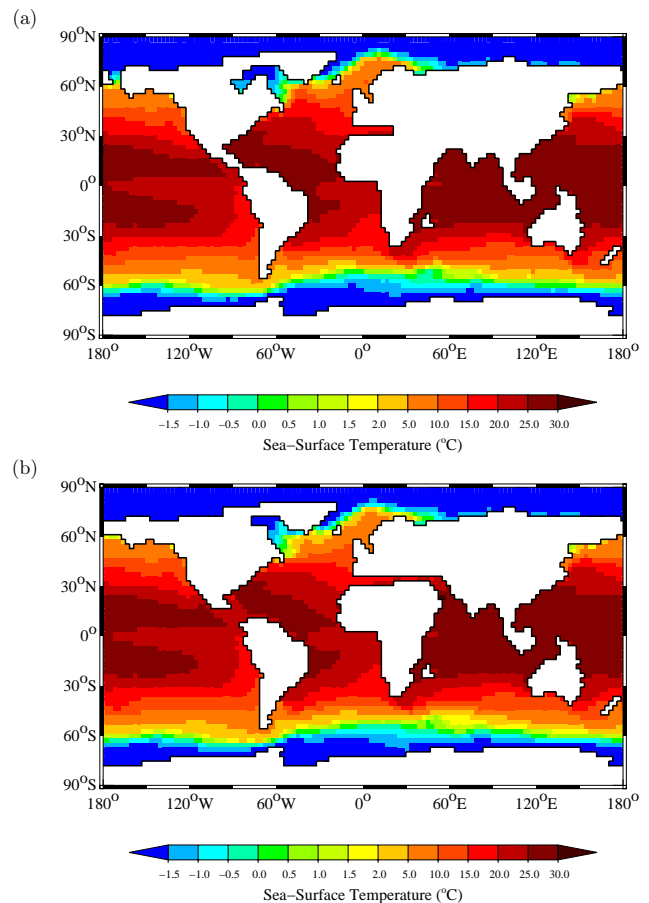


Fig. 1. Initial sea-surface temperatures for (a) the CTRL experiment and (b) the Miocene experiments. Grid elements with a temperature below -1.5°C are covered by sea-ice.

The slab model included in the Planet Simulator precludes the interactive calculation of circulation changes. Therefore, we prescribed the oceanic heat flux distributions for the preindustrial (used for the CTRL experiment) and the Middle Miocene (used for the Miocene experiments). The preindustrial oceanic heat flux distribution was calculated from a preindustrial experiment forced with the same boundary conditions as the experiment CTRL, but fixed sea-surface temperatures and sea-ice cover derived from the LSG preindustrial experiment. The differences between the sea surface temperatures calculated by the model and the ones prescribed determined the oceanic heat flux adjustments to apply to ocean grid-cells in order to mimic the heat transport by ocean currents at preindustrial. The same procedure was applied under Miocene boundary conditions used for experiment MM1 to obtain the oceanic heat flux distribution for the Middle Miocene. The oceanic heat fluxes obtained are shown in Fig. 2. The distribution of Miocene oceanic heat fluxes shows a weakening of the surface heat transfer to the North Atlantic due to the opening of the Central American

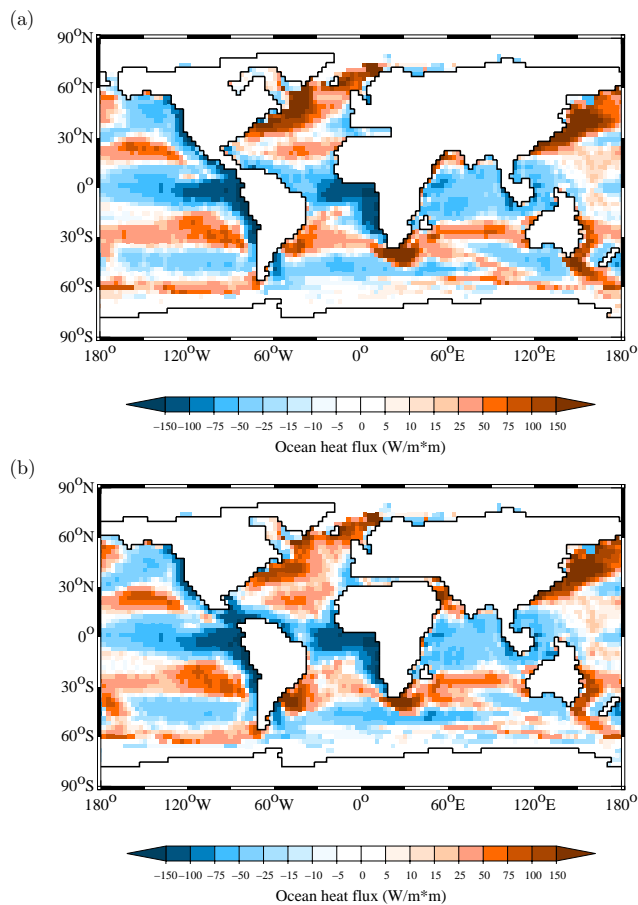


Fig. 2. Oceanic surface heat transfer for (a) the CTRL configuration and (b) the Miocene configuration. Positive values indicate a net transfer of heat from the ocean to the atmosphere.

Seaway, but an increase of the heat transfer to the South Atlantic. However, besides the reorganization of heat transfer in the Atlantic Ocean, the distribution of the surface heat fluxes at the Miocene does not differ much from the preindustrial distribution.

2.1.3 Land-sea distribution and topography

The use of LSG sea-surface temperatures as initial oceanic conditions imposed us to stick to the land-sea distribution and corresponding topography prescribed in the LSG experiments (Butzin et al., 2010). The control experiment was therefore forced with the present-day LSG land-sea mask and topography, whereas the Miocene experiments were forced with the Miocene LSG land-sea mask which takes into account an open Central American Seaway, an open Eastern Tethys Seaway, a filled Hudson Bay and a closed Bering Strait as stated above (see Fig. 3). However, the Miocene LSG simulations consider a present-day topography on land. It is thought that elevation on land was globally lower during the Miocene (Ruddiman, 1997; Harris, 2006; Gregory-

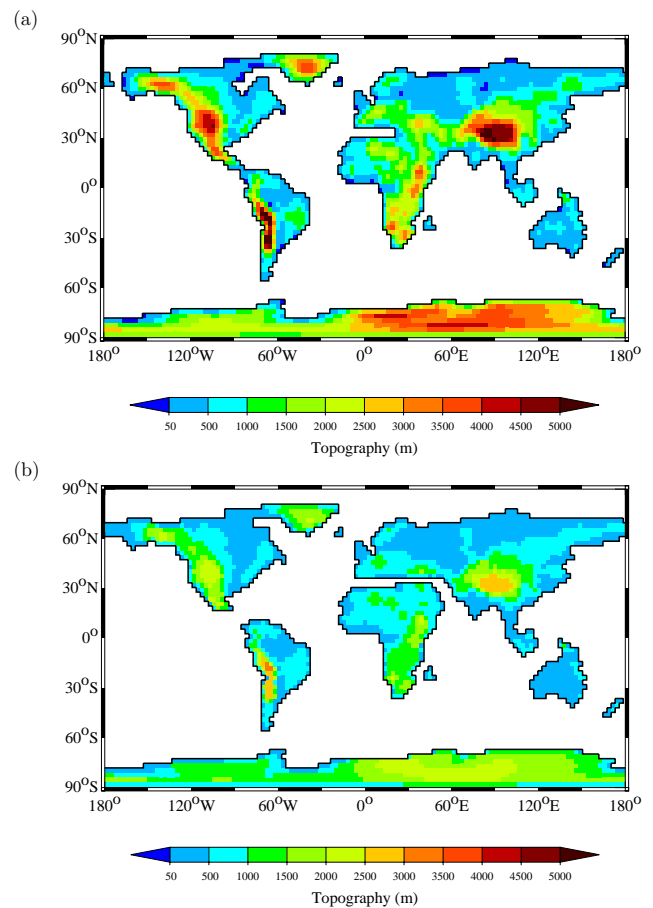


Fig. 3. Land-sea mask and topography on land for (a) the CTRL configuration and (b) the Miocene configuration.

Wodzicki, 2000). We therefore applied the algorithm described in Kutzbach et al. (1989) in order to reconstruct a topography approximately at half-height of its modern elevation.

$$h = 400 \text{ m} + (h_0 - 400 \text{ m})/2 \quad \text{where } h_0 \geq 400 \text{ m}$$

h_0 corresponds to the preindustrial topography and h to the Miocene lowered topography. That algorithm halves the elevation only above a base level of 400 m to approximate a geologic situation in which some continental relief was present prior to geologically recent uplift (Kutzbach et al., 1989). The present-day and Miocene land-sea mask and topography are shown on Fig. 3. A more precise study would have used the recent Middle Miocene paleotopographic reconstruction by Herold et al. (2008), geographically constrained at 15 Ma. Unfortunately, the LSG land-sea distribution is incompatible with the paleogeography of Herold et al. (2008), especially regarding ocean gateways, which are central to the present study. Nevertheless, our Miocene adapted topography agrees fairly well with the reconstruction of Herold et al. (2008), given the model resolution. The elevations of the North American, European and African reliefs are comparable to

the ones reported in Herold et al. (2008). However, the maximum elevation of the Tibetan Plateau is limited to 3500 m in our reconstruction, whereas Herold et al. (2008) constrained it to 4700 m. On the contrary, the Andes are around 500 m higher in our Miocene topography. Nevertheless, the differences between both topography reconstructions remain within the paleoelevation data errors for the Tibetan Plateau (Currie et al., 2005; Wang et al., 2006) and the Andes (Gregory-Wodzicki, 2000).

2.1.4 Vegetation cover

Surface boundary condition parameters controlled by the vegetation cover (surface albedo, roughness length and rooting depth) have been derived from equilibrium runs of the CARAIB model. The surface albedo, roughness length and rooting depth of the land grid-cells are calculated from the PFT abundances and specific albedo, roughness length and rooting depth values attributed to each PFT. To obtain the preindustrial vegetation parameters, we performed an equilibrium run of CARAIB, forced with 280 ppmv of CO₂ and the climatology of New et al. (2002). All of the experiments were forced with the preindustrial vegetation parameters except for experiment MM4-veg. In experiment MM4-veg, the vegetation parameters were replaced by their Middle Miocene distributions derived from an equilibrium run of CARAIB forced with 500 ppmv of CO₂ in the atmosphere and the climate from the experiment MM4, which is the warmest and most humid of the series and in best agreement with proxy-based climate reconstructions (see Sect. 4). We used the anomalies of the GCM climatic fields between the Middle Miocene (experiment MM4) and the preindustrial (experiment CTRL), added to the climatology of New et al. (2002), as climatic inputs for the Middle Miocene CARAIB simulation, following the approach described in Otto et al. (2002). The vegetation parameters of the emerging land-points from the Miocene land-sea distribution were extrapolated from the vegetation parameters of the nearby land-points, using an inverse distance weighted average procedure.

2.1.5 Atmospheric CO₂ concentration

We forced our simulations with various atmospheric CO₂ concentrations. The control experiment, as well as the first Miocene simulation experiments MM1 and MM2 used a preindustrial CO₂ level of 280 ppmv. In experiment MM3 the CO₂ concentration was set to 200 ppmv. 200 ppmv is within the range given by marine isotopic reconstructions suggesting low and constant CO₂ levels throughout the Miocene (Pagani et al., 1999; Henderiks and Pagani, 2008; Pearson and Palmer, 2000). For experiment MM4 we adopted a value of 500 ppmv to test the hypothesis of high CO₂ levels during the Miocene suggested by terrestrial proxies (Kürschner et al., 2008; Retallack, 2009).

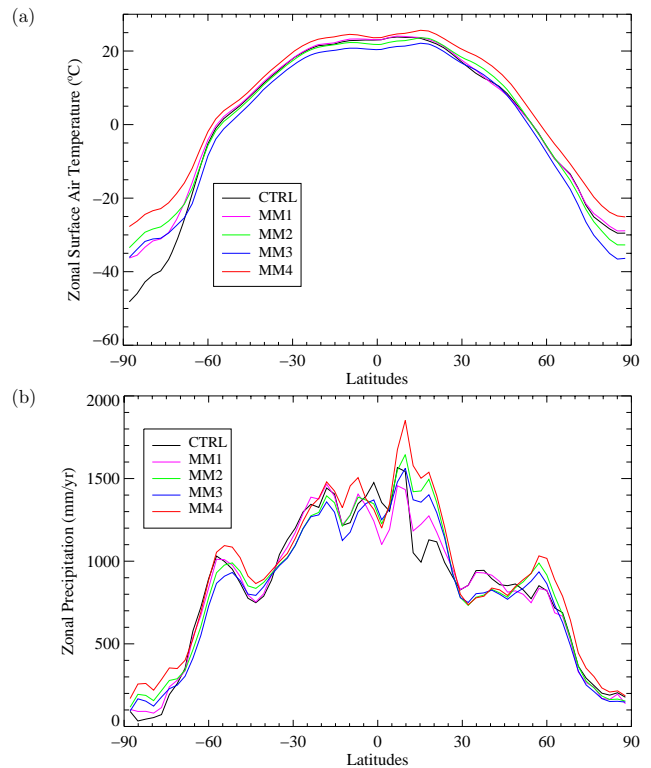


Fig. 4. Zonal average (a) surface air temperature (°C) and (b) precipitation (mm/yr) for the series of simulation experiments MM1 to MM4.

2.1.6 Orbital configuration

As we refer for the MMCO to a time span of about two million years integrated over several orbital cycles, we applied a present-day orbital configuration (eccentricity 0.016724°, obliquity 23.446° and longitude of perihelion 102.04°) and solar constant (1365 W/m²) for the whole series of experiments. To test the potential effect of such a warm orbital configuration on the MMCO climate we performed an additional experiment where we applied a cold LGM orbital configuration (eccentricity 0.018994°, obliquity 22.949°, longitude of perihelion 114.42° and present-day solar constant) under MMCO boundary conditions similar to those in experiment MM4. The “cold” orbital configuration induced a global temperature decrease of -0.1 °C in comparison to the “warm” present-day one, and essentially affected the oceanic grid-cells at high latitudes, due to the response of sea-ice to the reduction of insolation in winter. Because of this low sensitivity of the model to orbital forcing, we kept the present-day orbital configuration for the whole series of experiments.

Table 2. Global, continental and oceanic annual mean near-surface temperature T_{2m} ($^{\circ}\text{C}$) and precipitation (mm/yr) anomalies for the five Middle Miocene simulation experiments. The continental mean excludes the contribution from Antarctica since strong warming can be attributed due to the absence of ice that is not representative of the other effects on the continents. All results reported here are global means over the last 20 years of 50-year simulations, allowing 30 years for the model to equilibrate. The CTRL absolute values are shown for reference.

	T_{2m} ($^{\circ}\text{C}$)			Prc (mm/yr)		
	Global	Ocean	Continent	Global	Ocean	Continent
CTRL	12.3	15.3	11.6	1022	1138	803
Anomalies (EXPERIMENT-CTRL)						
MM1	+0.6	+0.5	-0.2	-5	+6	-38
MM2	+0.3	-0.5	+0.8	+20	+8	+38
MM3	-1.5	-2.1	-1	-14	-36	+28
MM4	+2.9	+2	+3.7	+73	+70	+85
MM4-veg	+3.4	+2.4	+4.3	+92	+74	+143

3 Results

3.1 Experiment MM1: surface ocean and ice-sheet boundary conditions

Experiment MM1 shows a global temperature increase of $+0.6^{\circ}\text{C}$ (see Table 2) that is mainly due to oceanic warming and Antarctic and Greenland warming in the absence of land-ice, whereas the temperatures and precipitation on other continents decrease. The zonal averages of surface air temperature (SAT) and precipitation are shown in Fig. 4. The zonal average temperature and precipitation anomalies (MM1-CTRL) are also shown in Fig. 5 to allow a finer comparison. The MM1 zonal temperature averages do not indicate large differences from the control experiment at any latitude, except at high latitudes of both hemispheres. The warming at high latitudes linked to an increase of precipitation is due to the absence of ice on land.

Figure 6 shows the annual mean surface air temperature (SAT) and precipitation anomalies between experiment MM1 and the control run CTRL. Large increases of the surface air temperature occur over Greenland and especially Antarctica. The absence of ice on Antarctica and Greenland strongly decreases the surface albedo that induces large warming and a decrease of the snow cover, leading to a positive albedo feedback during summer in each Hemisphere (not shown). However, in winter the influence of surrounding colder oceanic air masses induces a net cooling of about -1°C over Greenland. Large precipitation disruptions occur in the tropics and sub-tropics as well as over the North Atlantic Ocean.

Significant changes in surface air temperature as well as in precipitation are obtained especially over the oceans. These are a consequence of the sea surface temperature modification in response to ocean circulation changes in the Miocene LSG simulation. The reduction of the heat transfer to the

North Atlantic leads to large decreases of SAT in that region. Colder and drier conditions are obtained along the south-west coast of North America but the strongest decrease of SAT, of up to -6°C , occurs in the North Atlantic, along the south coast of Greenland. This region also experiences a large decrease of precipitation linked to the cooling of the air masses. The colder conditions over the North Atlantic induce continental temperature decreases together with precipitation increase, notably over northwestern Europe and Africa in winter. However, the decrease of precipitation of about -400 mm/yr over the northern part of South America and the east coast of North America, linked to a decrease of surface evaporation, leads to a surface temperature increase of more than 1°C .

The opening of the Central American Seaway and the closure of the Bering Strait, which inhibits the influx of fresh and cold water from the Arctic Ocean into the Pacific induces warming in the North Pacific, reaching $+4^{\circ}\text{C}$ along the west coast of North America together with a precipitation increase. This brings warmer and more humid air masses from the West to the Centre of North America and warmer air masses to the East after the passage of the high North American reliefs.

The opening of the Eastern Tethys Seaway influences the SAT in Central Asia and East Africa. A strong increase of SAT is obtained over the Tethys Seaway and is linked to the decrease of surface albedo and the large reduction of topography over the region due to the opening of the seaway. Precipitation is also strongly increased over the open seaway. As mentioned before, the opening of the Eastern Tethys Seaway weakly impacts on Indian Ocean heat transport. The western part of the Indian Ocean does not show any significant changes in SAT when compared to the CTRL experiment. The land points surrounding the open seaway experience colder conditions, except in the Indian peninsula. The SAT decreases can be attributed to the more humid conditions that

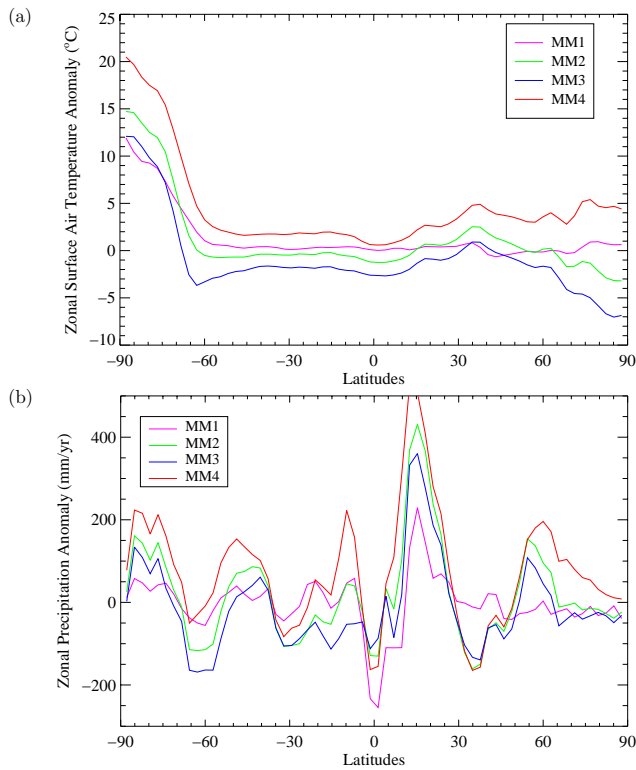


Fig. 5. Zonal average (a) surface air temperature anomalies ($^{\circ}\text{C}$) and (b) precipitation anomalies (mm/yr) for the series of Middle Miocene simulation experiments MM1 to MM4.

prevails in the presence of an open Tethys Seaway. However, since precipitation is strongly decreased in India during summer, the warming in this region can be linked to a reduced monsoon activity in presence of an open Eastern Tethys Seaway. Strong decreases of precipitation also occur in Indonesia and South-East China, suggesting a reduced monsoon activity in these regions too. Finally, the SAT cools by about -2°C in eastern Russia, extending the cooling trend over Europe to the east.

3.2 Experiment MM2: topography

The reduction of the topography in experiment MM2 generates the weakest effect in magnitude on global temperature in our series of experiments. It causes a global mean cooling of -0.3°C relative to experiment MM1, if we assume that the topographic and oceanic boundary conditions effects are independent of each other. However, the reduction of the topography significantly increases precipitation, especially on the continents (see Table 2). The lowering of the topography leads to a global decrease of temperature over the oceans whereas it leads to an increase of temperature over the continents. These opposite temperature effects over the oceans and continents can be explained by the conservation of the mass of the atmosphere in our model. The lowering of

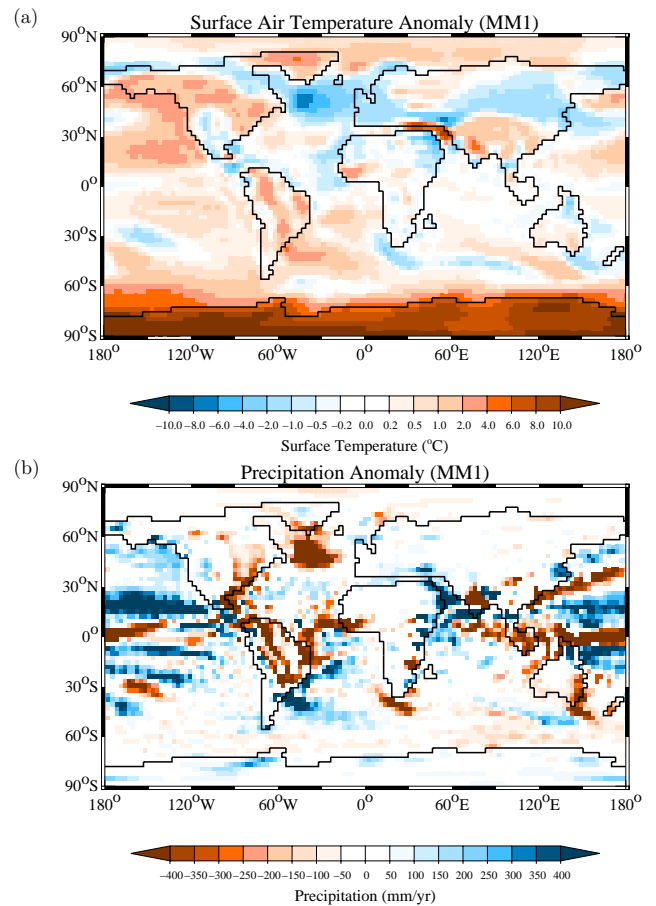


Fig. 6. (a) Annual mean surface temperature and (b) precipitation anomalies (MM1-minus-CTRL) for experiment MM1. Only the precipitation anomalies greater than one standard deviation for the long-term annual mean over the last 20 simulation years are shown.

the topography induces a surface pressure increase on land that leads to a surface pressure decrease over the oceans that in turn cools the oceans. Nevertheless, local surface pressure changes occur due to the displacement of high/low pressure cells in response to topography reduction. The lowering of the topography also produces localized warming, notably over Antarctica and around 30°N over the lowered reliefs. However, it decreases the temperatures at latitudes higher than 60°N (see Fig. 4). The lowering also decreases precipitation around 30°N but strongly increases precipitation especially in the tropics around the ITCZ (see Fig. 5).

As shown in Fig. 7, strong and localized warming occurs in the location of the present-day high reliefs that are directly affected by the largest topography reduction. Altitude reductions of more than 1000 m in some areas increase the annual mean SAT by more than $+10^{\circ}\text{C}$, e.g., in some parts of the Tibetan Plateau, the Andes, the Rockies, Greenland and Antarctica. In contrast to the continental warming, the SAT decreases over the oceans. The topography reduction

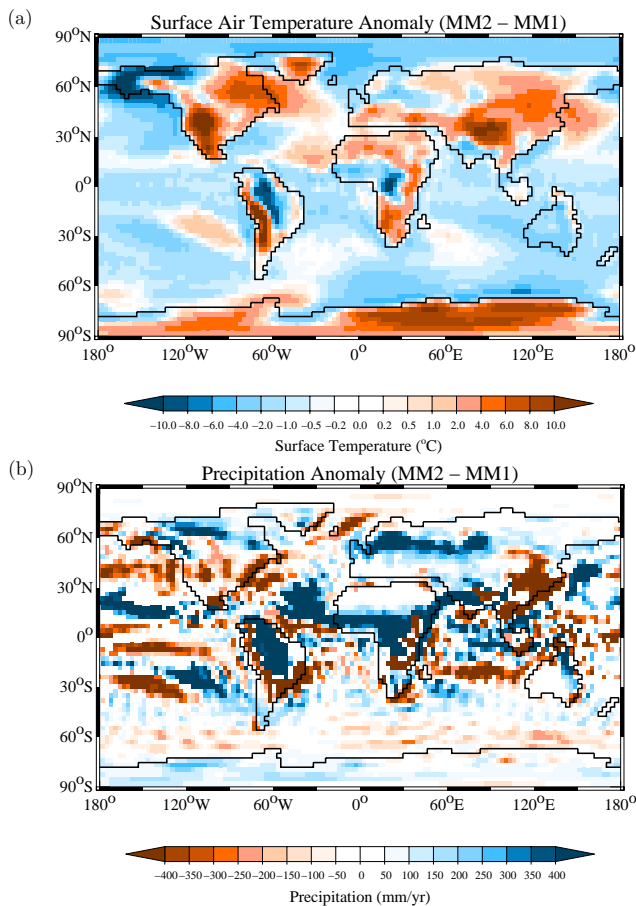


Fig. 7. (a) Annual mean surface temperature and (b) precipitation anomalies between experiments MM2 and MM1. Only the precipitation anomalies greater than one standard deviation for the long-term annual mean over the last 20 simulation years are shown.

also strongly disturbs the annual precipitation anomaly distribution on the continents (see Fig. 7). The anomalies show large differences when compared to the anomalies in experiment MM1. Northern and western Europe experience a SAT decrease that extends to the east. The annual anomaly essentially reflects the colder conditions that affect Eurasia in summer, whereas warmer conditions prevail in winter (see Fig. 8). Precipitation also strongly increases over northern Europe especially in summer (see Fig. 9). As illustrated in Figs. 10 and 11, showing respectively the summer and winter low-level winds (850 hPa) for experiments CTRL and MM2, seasonal effects can be due to a more zonal atmospheric surface circulation in the presence of lower reliefs. Therefore stronger and more direct winds from the North Atlantic flow across Europe and penetrate deeper into the continent, bringing more humid and colder conditions in summer and more humid and warmer conditions in winter, weakening the seasonal contrast of temperature and precipitation over Europe. This strong effect of the lower reliefs on the precipitation

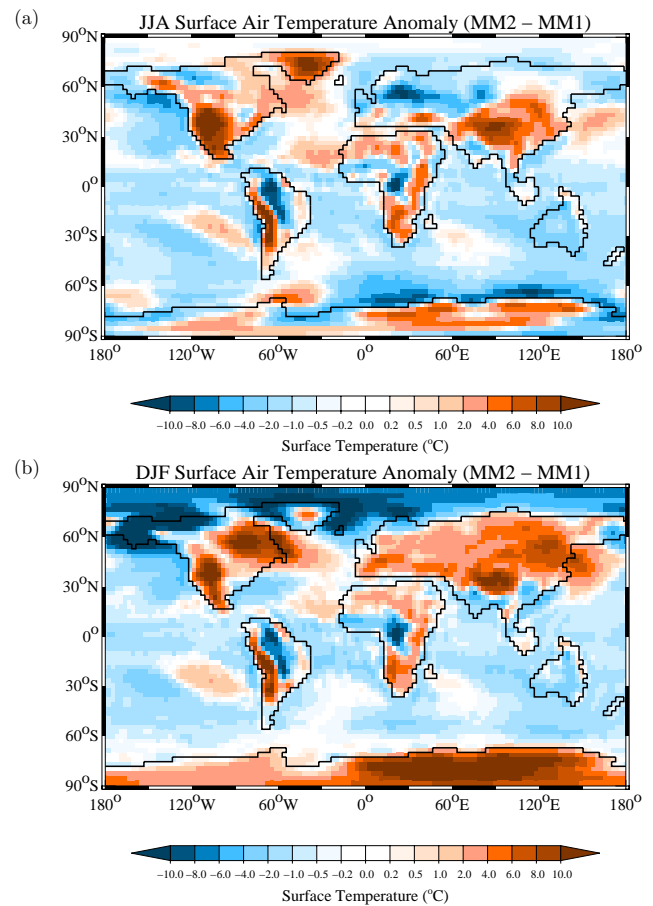


Fig. 8. Surface air temperature anomalies in (a) Northern Hemisphere summer (JJA) and (b) Northern Hemisphere winter (DJF) between experiments MM2 and MM1.

distribution in northern Europe is discussed in more detail in Sect. 3.2.1. Westerly winds coming from the North American continent instead of the Labrador Sea also flow over the North Atlantic, decreasing the activity of the Iceland low pressure cell. However, the southern part of Europe experiences an increase of SAT that is linked to the reduction of topography in the Alps and other reliefs, inducing local warming that dominates over the other effects. Furthermore, this warming can be reinforced in winter by a decrease of snowfall, resulting from the positive snow albedo feedback.

North America is affected by warming of more than $+2^{\circ}\text{C}$ that persists throughout the year. A precipitation increase in the North is induced by the direct contribution of humid air masses from the North Pacific especially in winter. In the absence of high reliefs, the winds flow directly to the west coast of North America and do not supply Alaska with humid air masses anymore. The isolation of the Alaska region leads to colder and drier conditions there in winter. The more zonal atmospheric surface circulation also contributes to isolate the Arctic Ocean that experiences strong winter cooling. In the

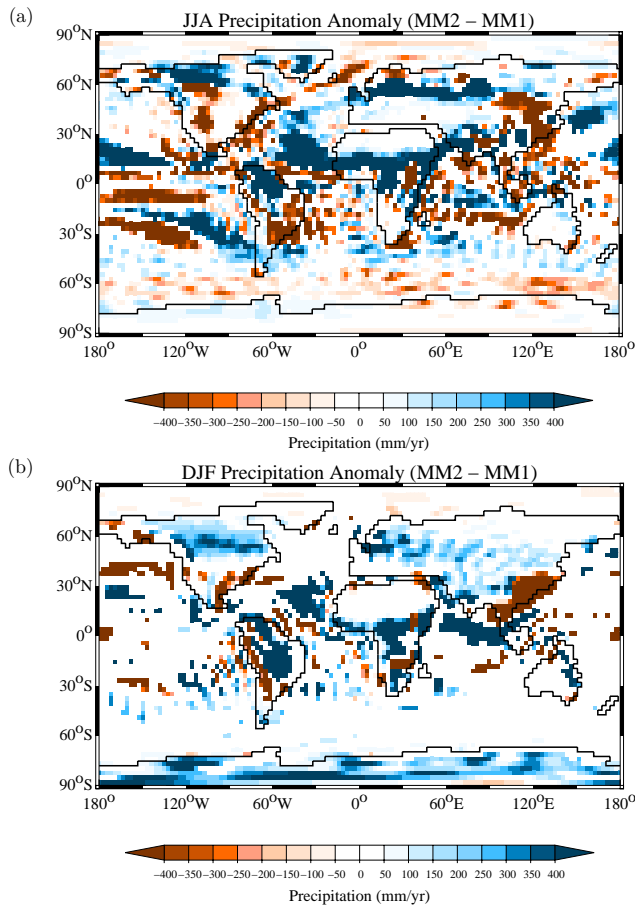


Fig. 9. Precipitation anomalies in (a) Northern Hemisphere summer (JJA) and (b) Northern Hemisphere winter (DJF) between experiments MM2 and MM1.

Centre of North America, the lower Rockies also weaken the frontal zone activity in summer between air masses coming from the West and the East. This leads to a decrease of surface evaporation that decreases precipitation in summer and contributes to warm the region.

The decrease of the height of the Tibetan Plateau also produces large seasonal impacts. SAT increases for the whole year over China and eastern Russia, but decreases over India, Indonesia and Australia. As expected, a lower Tibetan Plateau contributes to weaken the Asian monsoon activity, which is characterized by a decrease of precipitation in summer. The summer precipitation also decreases in Indonesia and the eastern Equatorial Pacific, where the surface winds weaken. North-East China gets drier during the whole year, due to a strengthening of the continental winds coming from the North-East in winter, but a decrease of the South-East winds in summer, which bring less humidity.

Africa is affected by an increase of SAT that can be directly attributed to the topographic reduction in the North and the South-East. However, SAT decreases in West and

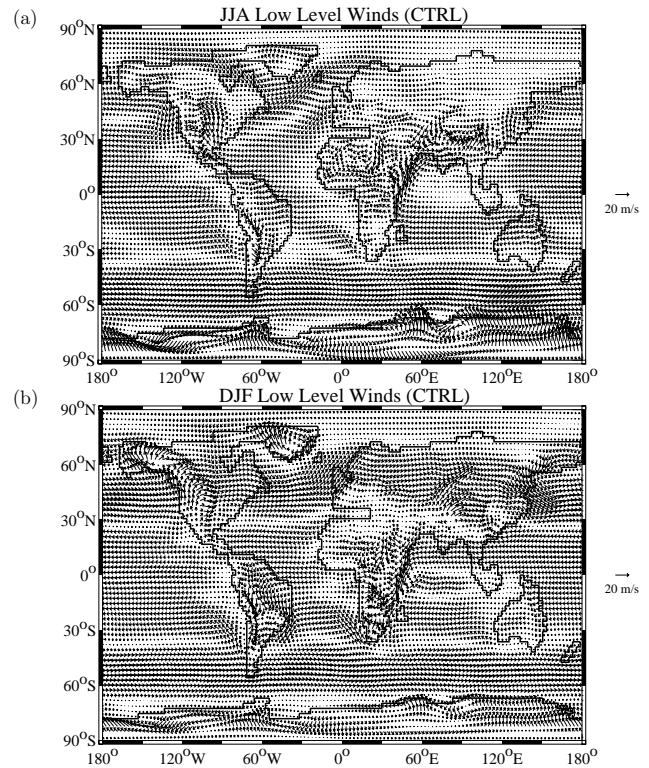


Fig. 10. Low-level winds (850 hPa) for the CTRL experiment in (a) Northern Hemisphere summer and (b) Northern Hemisphere winter.

Central Africa. This last effect comes together with a strong increase of precipitation, that can be attributed to the deeper penetration of westerly winds from the Atlantic together with a deeper penetration of north-easterly winds, which come from the moist region of the open Eastern Tethys Seaway. The northern part of South America also experiences a decrease of SAT together with a strong increase of precipitation.

3.2.1 Effects of the topography on precipitation in Europe

The lowering of the high reliefs leads to a strong increase of precipitation together with a SAT decrease from north-western to northeastern Europe. This is essentially a summer effect and is linked to a modification of the summer surface wind strength and direction. In order to determine the single most important topography change responsible for the precipitation disruption in Europe, we carry out several variants of experiment MM2, lowering separately and together the North American and European reliefs. We run three additional sensitivity experiments, reducing the topography in Europe (between 15° W and 30° E and 25° N to 75° N – experiment MM2-E), in North America (between 165° W and 60° W and 15° N to 75° N – experiment

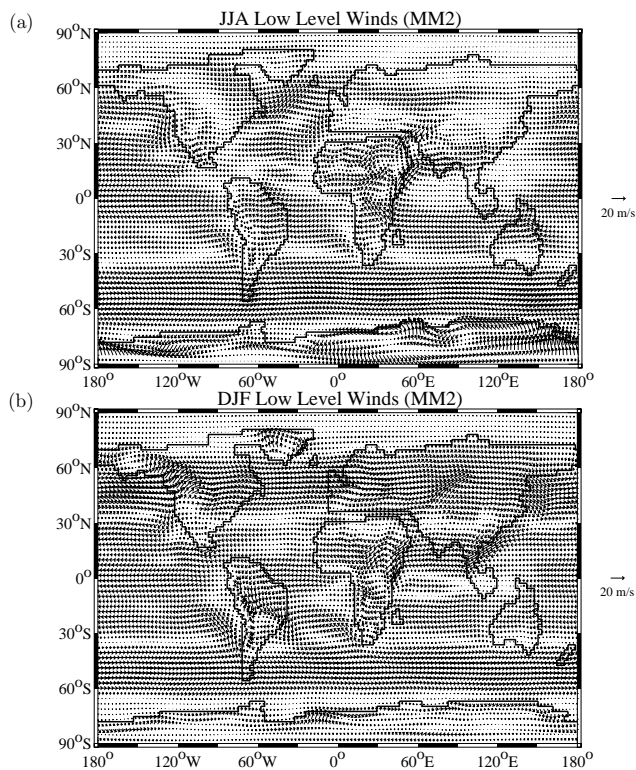


Fig. 11. Low-level winds (850 hPa) for the MM2 experiment in (a) Northern Hemisphere summer and (b) Northern Hemisphere winter.

MM2-A) and both together (experiment MM2-AE). We only lower the North American and European reliefs for this series of tests. The other reliefs are hold at their respective present-day elevations.

The disruption of summer precipitation and the summer winds at 850 hPa in the absence of European reliefs are shown in Fig. 12. The lower reliefs in North Europe allow stronger westerly winds that come more directly from the Atlantic Ocean to penetrate deeper into the continent, bringing more humid and cold oceanic air masses to northern Europe. Nevertheless, the lowering of the North European reliefs alone is not sufficient to form the wet tongue that we obtained in experiment MM2.

The lowering of the North American reliefs also produces stronger and more direct summer westerly winds in north-western Europe, generating more precipitation in the region (see Fig. 13). However the presence of the North European reliefs stops the wetter air masses coming from the West, and does not allow the wet tongue obtained in experiment MM2 to form neither. Precipitation increases in north-western Europe similar in terms of magnitude to those found in experiment MM2 are only obtained when the effects of European and North American topography changes are combined (Fig. 14). We also perform additional sensitivity experiments testing separately the effects of the lowering of the

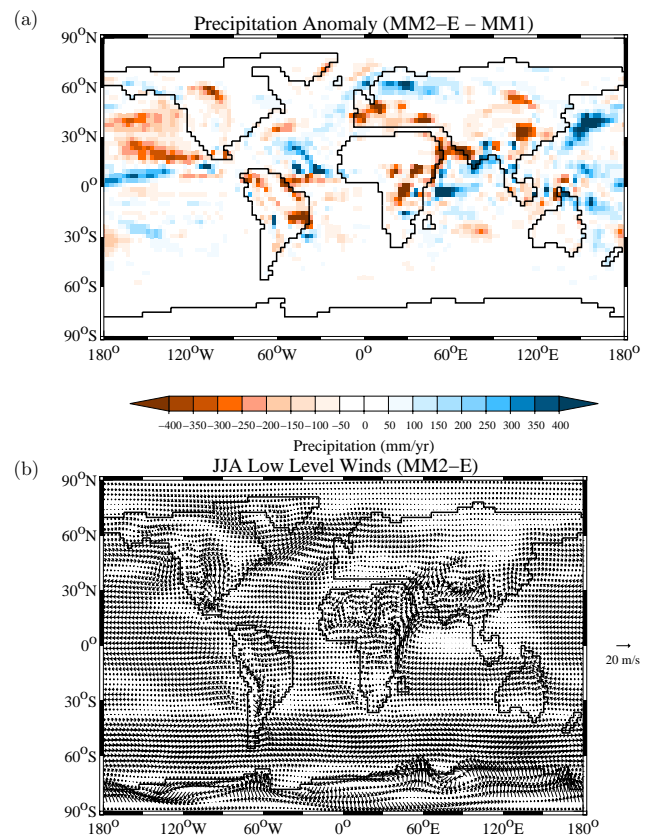


Fig. 12. (a) Annual mean precipitation anomalies (MM2-E-MM1) and (b) Northern Hemisphere summer low-level winds (850 hPa) for experiment MM2-E that considers a reduced topography only in Europe.

Tibetan Plateau, African reliefs and South American reliefs on the precipitation distribution in Europe. Effects on European precipitation and teleconnections found in these later experiments are rather weak (not shown). We conclude that the reduction of topography in North America and Europe is necessary to produce the colder and wetter conditions that prevail in North Europe in experiment MM2. However, the wet tongue does not extend to the East as far as it does in experiment MM2. We can therefore attribute the increase of precipitation in North West Asia to the reduction of the topography in Asia.

3.3 Experiment MM3: low CO₂

The lowering of the atmospheric CO₂ concentration in experiment MM3 produces a global cooling together with a precipitation reduction (see Table 2). The reduction of atmospheric CO₂ also reinforces the general cooling trend and decreases the precipitation at all latitudes as compared to the results of experiment MM2 (see Fig. 4). However, it does not disrupt the zonal profiles of SAT and precipitation. The surface air temperature and precipitation anomalies between

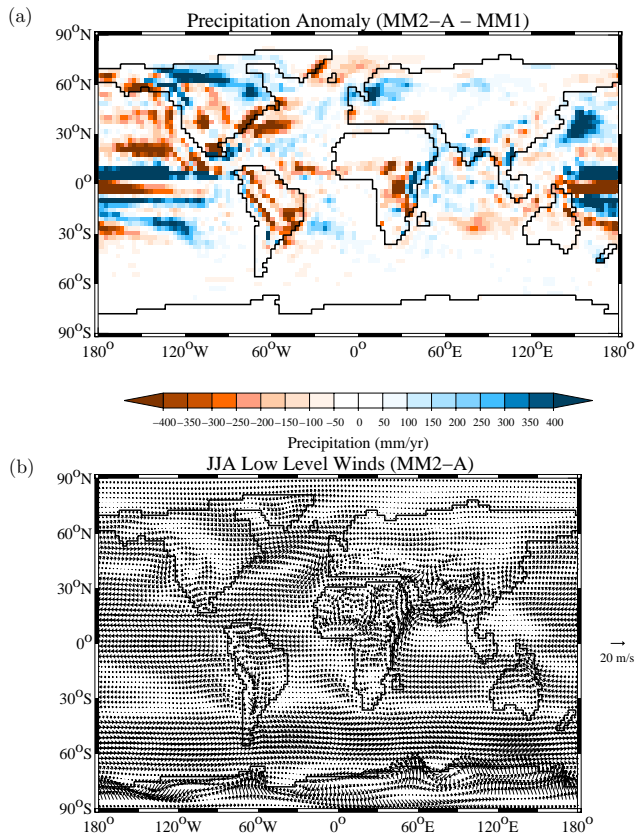


Fig. 13. Same as Fig. 12 for experiment MM2-A that considers a reduced topography only in North America.

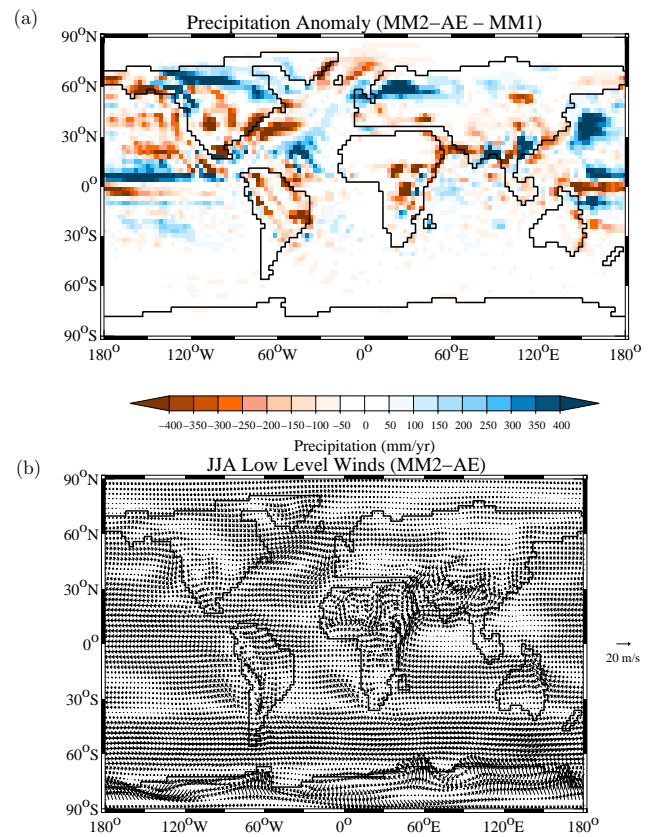


Fig. 14. Same as Fig. 12 for experiment MM2-AE that considers a reduced topography only in North America and in Europe.

experiments MM3 and MM2 are shown in Fig. 15. The 80 ppmv lowering of the CO₂ concentration induces a rather uniform temperature cooling of about -2°C . The magnitude of the cooling is similar over continents and oceans, and in both Northern and Southern Hemispheres. Stronger cooling occurs at high latitudes, especially over the Arctic and Antarctic Oceans, due to sea-ice feedback. The decrease of the CO₂ concentration does not disrupt the precipitation distribution when compared to experiment MM2. It slightly decreases the precipitation over the tropical oceans.

3.4 Experiment MM4: high CO₂

The increase of the atmospheric CO₂ concentration to 500 ppmv in experiment MM4 has the strongest effect on temperature of the series. It warms the global climate by $+2.6^{\circ}\text{C}$. The higher CO₂ level also reinforces the increase of precipitation caused by the reduction of the topography, producing the strongest effects of the four experiments on precipitation. The increase of atmospheric CO₂ reinforces the warming at high latitudes, reducing again the latitudinal temperature gradient (see Fig. 4). This high-latitude warming can be attributed to the melting of sea-ice under warmer conditions. The CO₂ induced warming also contributes to

increase the precipitation rate at all latitudes. The difference in surface air temperature between experiments MM4 and MM3, equal to $+4.4^{\circ}\text{C}$, corresponds to the climate sensitivity of the model to a CO₂ increase of 300 ppmv under Middle Miocene conditions. Thus, the Miocene sensitivity to a doubling of CO₂ must be of the order of 3.3°C (using the temperature increase between experiment MM4 and MM3 as a reference), if we assume that the global mean temperature variation is proportional to the radiative forcing (Forster et al., 2007), and radiative forcing is proportional to the logarithm of $p\text{CO}_2$ ratios (Myhre et al., 1998). In comparison, we obtained a climate sensitivity to a doubling of CO₂ from a preindustrial level of 280 ppmv to 560 ppmv of $+4.5^{\circ}\text{C}$ under a present-day configuration. The model climate sensitivity is thus significantly smaller under Middle Miocene conditions. That could be partially explained by the reduction of the sea-ice extent at Middle Miocene, which is very sensitive to CO₂ changes in our model.

The surface air temperature and precipitation anomalies between experiments MM4 and MM2 are shown in Fig. 16. The increase of the atmospheric CO₂ concentration in experiment MM4 leads to uniform temperature increases on the continents and the oceans in both hemispheres. The effect of CO₂ is larger than the effect of the topography

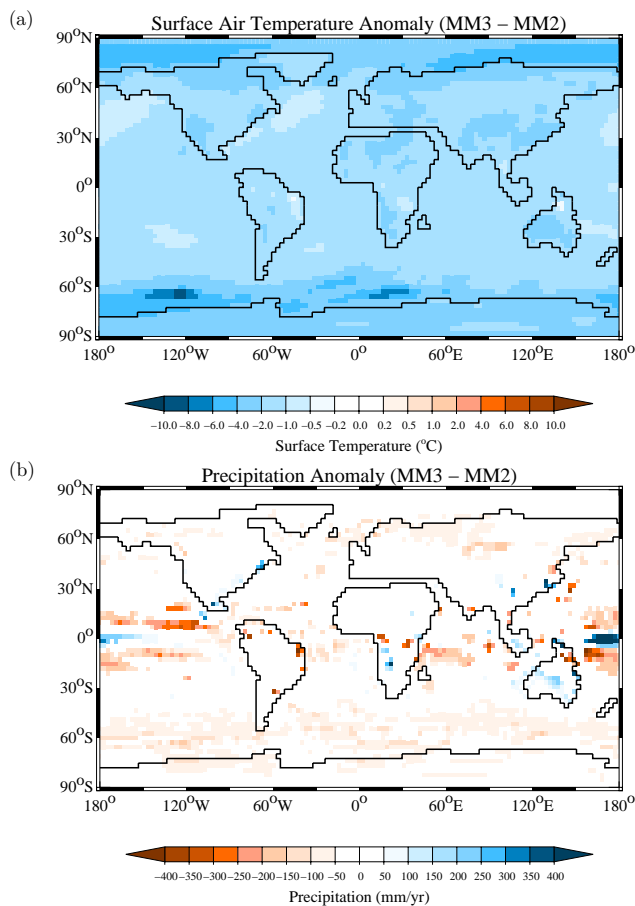


Fig. 15. (a) Annual mean surface temperature and (b) precipitation anomalies between experiments MM3 and MM2.

in some regions. Northwestern Europe notably experiences significant increases of temperature in experiment MM4, whereas the reduced topography alone induced a cooling in that region (see Sect. 3.2.1). The higher CO₂ concentration also produces a stronger warming at high latitudes and especially over the Arctic and Southern Oceans due to the melting of sea-ice. However, the higher CO₂ concentration does not disturb the precipitation distribution induced by the reduction of the topography in experiment MM2. The distributions of the precipitation anomalies are quite similar in experiments MM2 and MM4. The CO₂ effect reinforces the precipitation increases especially in the tropics.

3.5 Experiment MM4-veg: vegetation

The warmer and more humid conditions prevailing in experiment MM4 could lead to significant vegetation cover modifications that could in turn affect the climate. Here, we analyse the results of experiment MM4-veg, taking into account the vegetation changes in response to the MM4 climate, in order to quantify the order of magnitude and the local impacts of vegetation changes on the MMCO climate.

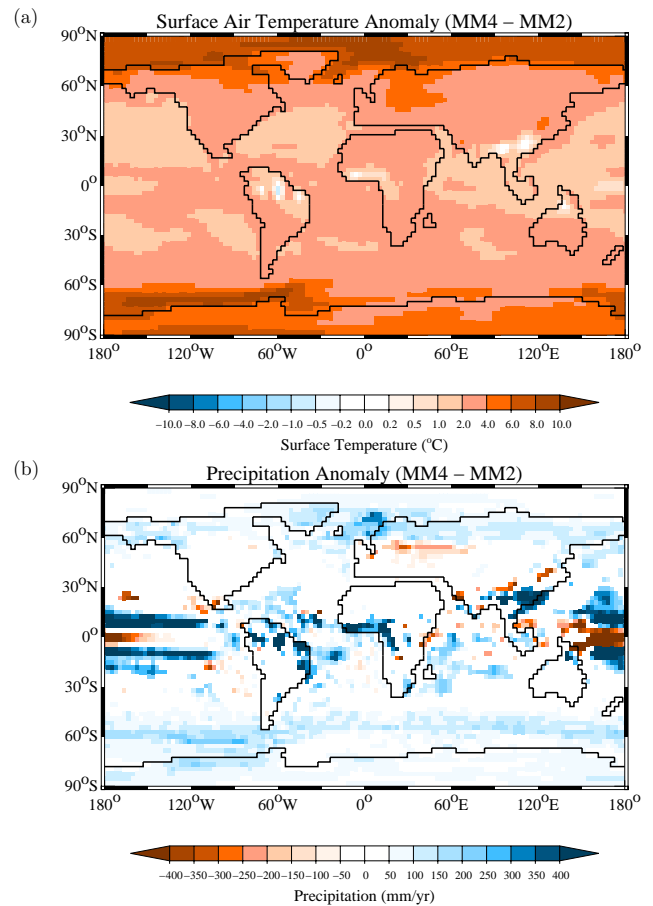


Fig. 16. (a) Annual mean surface temperature and (b) precipitation anomalies between experiments MM4 and MM2.

The vegetation distribution obtained with CARAIB from the climate of experiment MM4 is shown in Fig. 17 and compared to the preindustrial vegetation distribution used in the rest of the experiments. It should be noticed that the vegetation maps do not show Antarctica, because the New et al. (2002) climatology does not include any data point in Antarctica. Globally, in response to the warmer and more humid climate in experiment MM4, the simulated Miocene vegetation distribution demonstrates an expansion of forest biomes at the expense of grasslands and deserts. Tundra and temperate forests expand at high latitudes mainly at the expense of polar deserts. Deserts and semi-deserts are strongly reduced and replaced by grasslands or warm and open woodlands, especially in Central Asia where deserts completely disappear. Thermophilous types included in the subtropical forest biome expand particularly in South and Central Europe, due to the warmer and wetter conditions prevailing in the region. This result seems to be consistent with the reconstruction of Utescher et al. (2007), which suggests the presence of warm mixed and broadleaved evergreen forests in South and Central Europe. However, the drier conditions

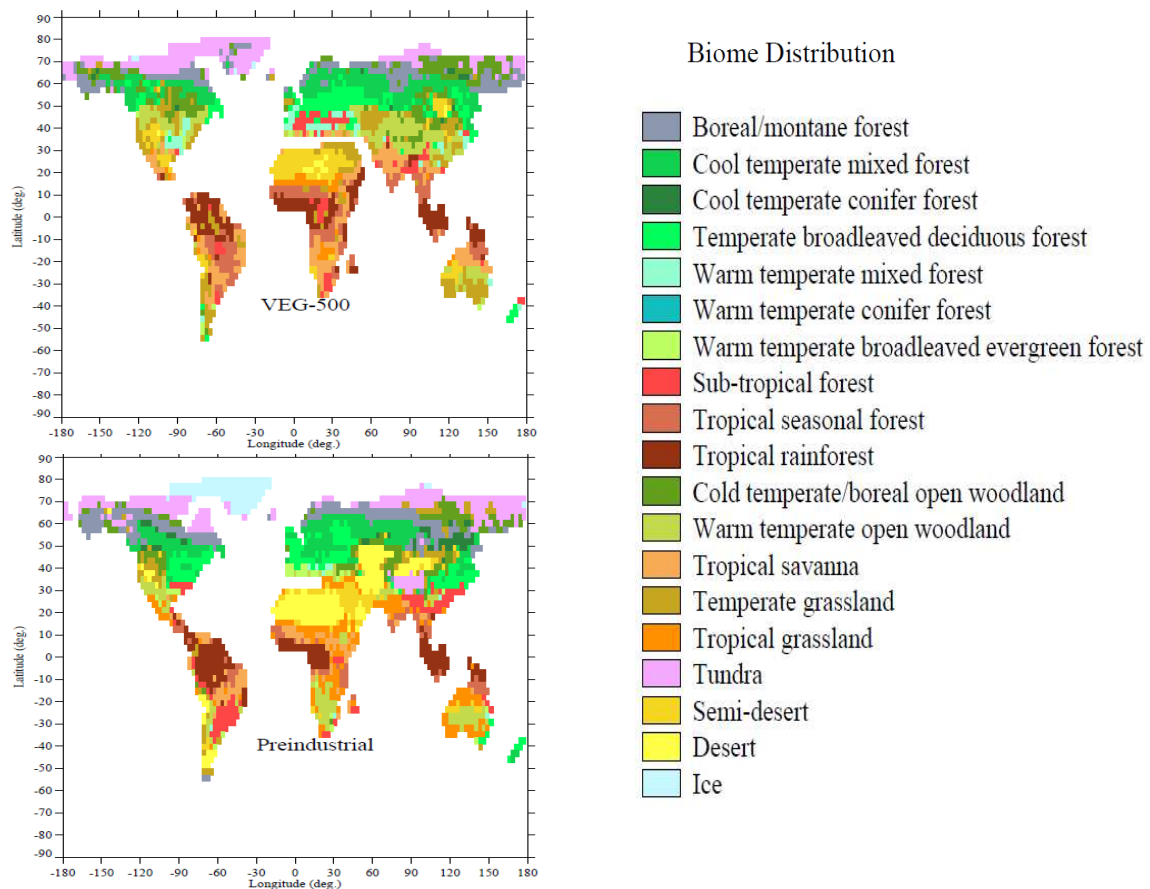


Fig. 17. Biome distributions from CARAIB preindustrial and MMCO equilibrium runs.

at the east coast of North America and in Southeastern China lead to the replacement of subtropical forests by warm and open woodlands.

The anomalies between experiments MM4-veg and MM4 are shown in Fig. 18 in order to isolate the vegetation effects from the other forcings applied in experiment MM4. Globally, experiment MM4-veg shows the strongest global temperature and precipitation increases of the series of Miocene experiments (see Table 2), especially on the continents due to the vegetation change impact. In comparison with experiment MM4 the vegetation changes produce an additional global warming of $+0.5^{\circ}\text{C}$ ($+0.4^{\circ}\text{C}$ over the oceans and $+0.6^{\circ}\text{C}$ over the continents) and an increase of precipitation of $+19\text{ mm/yr}$ ($+4\text{ mm/yr}$ over the oceans and $+58\text{ mm/yr}$ over the continents). Locally, the vegetation contribution is only slightly lower in terms of magnitude than the contributions of topography and high atmospheric CO_2 level. As described in Sect. 2, vegetation cover changes affect surface albedo and roughness length, but the albedo impact on surface temperature is dominant, because of its direct impact on the energy balance (Henrot, 2007). The changes in rooting depth mainly affect the water cycle and therefore precipitation. The differences between the surface albedo and rooting

depth derived from the Miocene and the preindustrial vegetation distributions are shown in Fig. 19.

Locally, the vegetation change effects on temperature are larger over the continents, than over the oceans (see Fig. 18). Only the Arctic Ocean experiences a warming of the same order due to the melting of sea-ice induced by the warming of the surrounding continental grid points. Strong warming occurs around the Eastern Tethys Seaway. It is due to the decrease of surface albedo (see Fig. 19) produced by the replacement of deserts and semi-deserts by open woodlands, which develop in the more humid conditions produced by the opening of the seaway. Central Asia also experiences a decrease of surface albedo linked to the replacement of deserts by forests. SAT increases in South and Central Europe due to the development of subtropical forests with a lower albedo. However, SAT decreases in the Centre and South of North America as well as in Northeastern China. This effect is linked to the increase of surface albedo induced by the opening of the landscape in response to the reduction of precipitation in these regions obtained in experiment MM4. Precipitation is essentially affected by vegetation changes in the tropical regions. The development of forests around the Eastern Tethys Seaway increases the soil water content (see Fig. 19)

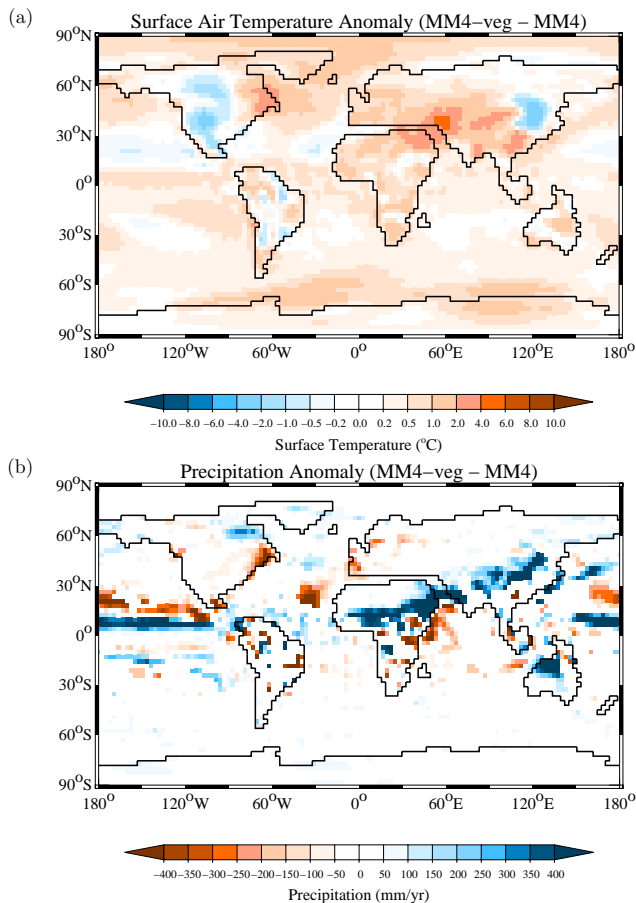


Fig. 18. (a) Annual mean surface temperature and (b) precipitation anomalies between experiment MM4-veg and MM4.

leading to an increase of evaporation and precipitation. The same effect occurs in central Asia. The precipitation increase in Equatorial Africa is due to the expansion of the tropical forests which enhances the hydrological cycle. The precipitation decrease along the west coast of Europe is due to the replacement of temperate forests by open woodlands, which decreases the soil water content.

4 Discussion

In our series, experiment MM1 assesses the climatic effects of the MMCO surface ocean heat flux distribution, derived from Miocene LSG model simulation (Butzin et al., 2010). These changes produce contrasted effects on surface air temperature and precipitation over the oceans that influence the climatic conditions on land. The reduction of the oceanic heat transfer to the North Atlantic due to the opening of the Central American Seaway brings colder conditions over the North Atlantic and northwestern Europe. This effect agrees with the majority of published modelling studies results indicating that the closure of the Central American Seaway was

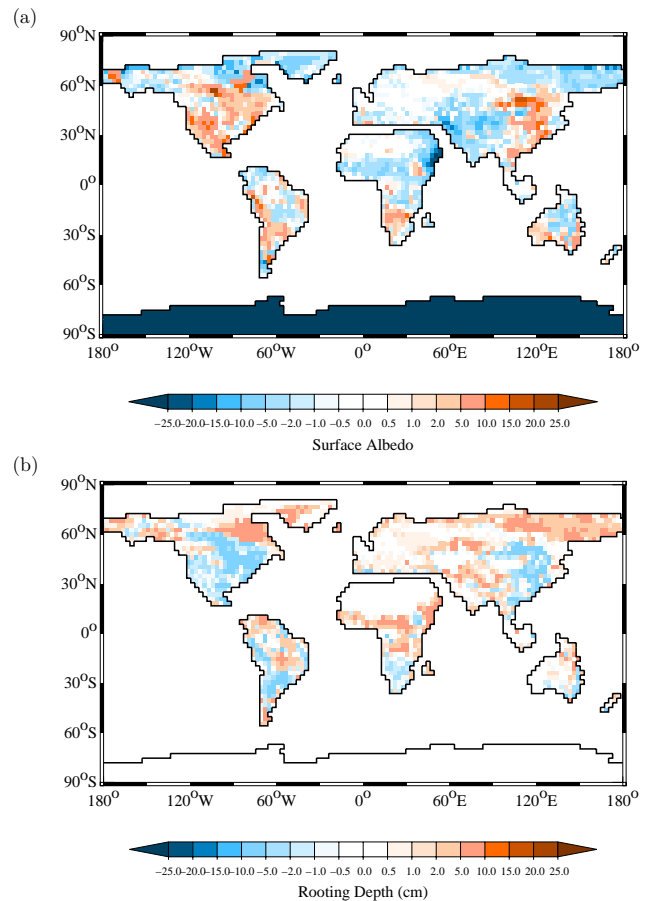


Fig. 19. (a) Surface albedo difference and (b) rooting depth difference between experiment MM4-veg and CTRL.

responsible for increased oceanic heat transport to the North Atlantic that brought warmer conditions and ultimately increased precipitation in the Northern Hemisphere (Lunt et al., 2008; Schneider and Schmittner, 2006). The decrease of precipitation in South Asia, linked to SST changes, indicates a weakening of the Asian monsoon. According to Tschuck et al. (2004), the weakening of the Asian monsoon can be linked to the increase of sea surface temperatures in the equatorial Indian Ocean and western Pacific Ocean. Therefore, the warmer conditions induced in the Pacific by the opening of the Central American Seaway may be contributing to the reduction of the precipitation in some parts of Asia.

Experiment MM2 allows us to discuss the climatic effects of the reduced topography on land. It also represents a Middle Miocene state with a preindustrial CO_2 concentration of 280 ppmv, since experiment MM2 includes all of the Middle Miocene boundary conditions considered in this study. As already demonstrated by Kutzbach et al. (1989), the reduction of the topography allows a more zonal atmospheric circulation and the westerly flow to continue over the lowered Plateaus at mid-latitudes, e.g., the Colorado Plateau,

the Tibetan Plateau and European reliefs. Moreover, the reduced height of the Tibetan Plateau prevents the development of a monsoon-like circulation (Kutzbach et al., 1989; Harris, 2006) that induces a strong decrease of precipitation in East Asia. Recently, Herold et al. (2009) focused on the effect of lowered Tibetan Plateau and Andes on the Middle Miocene climate using the NCAR model (CAM v.3.1) and Community Land Model (CLM v.3.0) coupled to a slab ocean model with fixed sea-surface temperatures. Herold et al. (2009) also obtained strong local warming and a significant disruption of the surface winds due to the reduction of elevation over the Tibetan Plateau. However, the prescription of fixed sea-surface temperature in their experiment precluded a response of the ocean and therefore of the Asian monsoon system. Nevertheless, they also pointed out that the lowering of the Tibetan Plateau leads to a cooling linked to snow depth increase in Central Eurasia. In our experiment MM2, the reduction of the topography leads to slight warming in Eurasia, and does not significantly alter the snow depth in the region. Therefore, we can attribute the Eurasian warming in our results to the local increase of temperature induced by the reduction of reliefs higher than 400 m in the region. Unfortunately, our setup does not allow us to isolate the influence on Eurasia of the Tibetan Plateau elevation change. The lowering of North American and European reliefs produces wetter and colder conditions over northwestern Europe that are in disagreement with proxy-based reconstructions of the European Middle Miocene climate (Mosbrugger et al., 2005). However, the reduction of the seasonal gradient and the warming in South and Central Europe agree well with several reconstructions of the Middle Miocene climate based on pollen analysis (Jimenez-Moreno and Suc, 2007) and mega- or microfloral records (Mosbrugger et al., 2005; Utescher et al., 2007). Moreover, the reconstruction of Utescher et al. (2007) and other reconstructions based on the analysis of small mammals (Van Dam, 2006) showed evidence for the persistence of a European wet zone during the Miocene, in agreement with our results. Nevertheless, the maximum increases of precipitation are located further north in Europe where no proxy reconstruction is available.

In the next two experiments (MM3 and MM4) we test the effect of various CO₂ concentrations on the middle Miocene climate. The CO₂ effect is rather uniform on the continents and the oceans of both hemispheres. However, the combination of the CO₂ and topographic effects in experiment MM4 generates a stronger warming over the continents than over the oceans, which is also seen in the results of Tong et al. (2009). The results of experiment MM4 over northwestern Europe show a slight increase of temperature, since the topography induced effect cooled that region. Both the topography reduction and increased CO₂ concentration contribute to wetter and warmer conditions in Europe, in better agreement with the proxies reconstructions (Mosbrugger et al., 2005; Utescher et al., 2007). As in Tong et al. (2009), the increase of the CO₂ concentration warms

the high latitudes reducing the latitudinal gradient and also increases the precipitation. The increase of the CO₂ concentration furthermore enhances the hydrological cycle in the tropics, according to Tong et al. (2009). Nevertheless the activity of the monsoon system is still reduced in experiment MM4. This confirms the dominant effect of topography on the Asian monsoon system as compared to the CO₂ contribution (Tong et al., 2009).

Experiment MM4-veg finally allows us to investigate the vegetation feedback on climate in response to a warm and humid climate for the MMCO. The simulated vegetation distribution forced with the climate of experiment MM4 mainly demonstrates a reduction of the desert and sub-desert areas in the benefit of grasslands and forests, as well as an expansion of warm forest types poleward of the subtropical zone. This fairly agrees with the Middle Miocene database-based vegetation reconstruction used as boundary condition in the study of Tong et al. (2009), despite the differences in plant type classifications. Our vegetation distribution also agrees over South and Central Europe with the reconstruction of Utescher et al. (2007), which suggested the presence of warm mixed and broadleaved evergreen forests in South and Central Europe. Consistently with the data from Jimenez-Moreno and Suc (2007), CARAIB also yields warm and open mixed forest in Southwest Europe, whereas it leads to thermophilous and mesothermic elements in Central Europe. Such a change in the vegetation cover contributes to maintain and even to increase the warm and humid conditions that prevailed in experiment MM4.

In the series of sensitivity tests, several experiments result in an increase of the global surface air temperature. The increase of the atmospheric CO₂ concentration to 500 ppmv in experiment MM4 produces the strongest global warming of the series of four experiments, as compared to the warming produced by oceanic heat transport and ocean gateway changes (experiment MM1) or reduced topography (experiment MM2). A lower than preindustrial CO₂ concentration cools the global climate. A higher CO₂ concentration seems therefore necessary to generate a warmer climate in the Middle Miocene. The lower climate sensitivity of the climate model under Middle Miocene conditions may partly explain the requirement of the model for high CO₂ to produce significant temperature increases at the MMCO. However the warming we obtain is much lower than suggested by proxy data (Mosbrugger et al., 2005; Zachos et al., 2001), which witness temperatures at middle latitudes up to 6 °C higher than at present (Flower and Kennett, 1994). Nevertheless, our results agree fairly well with the results of previous modelling studies focusing on the Middle Miocene climate. Tong et al. (2009) tested the sensitivity of the Middle Miocene climate to various concentrations of atmospheric CO₂ using the NCAR model (CAM v.3.1) and Community Land Model (CLM v.3.0) coupled to a slab ocean model. They obtained a global warming of +0.6 °C for an atmospheric CO₂ concentration of 355 ppmv and a global warming of +2.9 °C for

an atmospheric CO₂ concentration of 700 ppmv in comparison to a present-day control run with a reference CO₂ concentration equal to 379 ppmv. You et al. (2009) used the same models to test the effect of various CO₂ concentrations together with several sea surface temperature gradients. They obtained temperature increases of +2.3 °C for an atmospheric CO₂ concentration of 350 ppmv and a high SST gradient and of +3.5 °C for CO₂ at 700 ppmv and a medium SST gradient. Micheels et al. (2009a) used the Planet Simulator to test the sensitivity of the Late Miocene climate (Tortonian) to various CO₂ concentrations. They obtained global warming between +2.3 °C for 280 ppmv and +3.7 °C for 460 ppmv in comparison to a preindustrial control run with a CO₂ concentration of 280 ppmv. In comparison to our results, Micheels et al. (2009a) found a greater warming under lower CO₂ concentration with the Planet Simulator. This effect could be due to the differences in the boundary conditions they used for the Late Miocene. They notably adopted a present-day ocean heat flux distribution, including a stronger Gulf Stream than used here and a lower topography on land in some regions. They also prescribed a vegetation distribution for the Late Miocene, where all the desert areas were replaced by forest or grassland ecosystems and the boreal forests shifted further North, whereas we did not consider any vegetation change in the MM1 to MM4 simulation experiments.

The model results consistently indicate that a higher than present-day CO₂ concentration is necessary to produce a warm Middle Miocene climate (You et al., 2009; Tong et al., 2009). In that sense, the model results support the terrestrial proxy reconstruction suggesting higher atmospheric CO₂ concentrations at the MMCO, between 300 and 850 ppmv (Kürschner et al., 2008; Retallack, 2009). Conversely modelling results do not support the low CO₂ concentration, between 140 and 300 ppmv, derived from marine isotopic records, that suggest a decoupling between CO₂ and temperature during the Middle Miocene (Henderiks and Pagani, 2008; Pearson and Palmer, 2000). Experiments using lower CO₂ concentrations generate colder climate than at present-day (experiment MM3 in this study, Tong et al., 2009 or You et al., 2009). However, as recently discussed by Pagani et al. (2010, Supplement) CO₂ concentrations during the Miocene could possibly have been higher than suggested by previous estimates based on planktonic foraminiferal $\delta^{18}\text{O}$ temperature reconstructions. Correcting for inherent biases could thus help to reconcile model results to proxy-based reconstructions. However, as emphasised by Diester-Haass et al. (2009), a high CO₂ level at the Middle Miocene would be difficult to reconcile with the high $\delta^{13}\text{C}$ values of benthic foraminifera, which suggest large deposition rates of organic carbon tending to reduce atmospheric CO₂ levels. Therefore model results should be interpreted with care.

We indeed do not take into account all the possible effects that could contribute to the Middle Miocene warm climate. We notably miss the feedback of climate on ocean circu-

lation at Middle Miocene, which could only be simulated with a fully coupled ocean-atmosphere model, since we used a slab ocean model as in previous studies (Tong et al., 2009; You et al., 2009). The opening of ocean gateways notably at low latitudes seems to have strongly contributed to modify the global ocean circulation in the Cenozoic in comparison to present-day (Bice et al., 2000; Von der Heydt and Dijkstra, 2008). We also only tested the effect of various CO₂ concentrations on climate given the large uncertainty in CO₂ estimations. We did not take into account a change in the concentrations of other atmospheric greenhouse gases such as methane. The potential role of such feedbacks is well illustrated by the results of our simulation experiment MM4-veg, which takes into account the feedback on climate from the changing vegetation cover compared to the first four simulation experiments of our series.

5 Conclusions

In this study, we examine the potential contributions of several boundary condition changes to the warm climate of the Middle Miocene and particularly the Middle Miocene Climatic Optimum (MMCO). We used the Planet Simulator, an Earth System model of intermediate complexity to investigate the contributions of the absence of ice on the continents, the opening of the Central American and Eastern Tethys Seaways, the lowering of the topography on land and the effect of various atmospheric CO₂ concentrations on the Middle Miocene climate. We also investigated the feedback of vegetation on climate. Therefore, we prescribe vegetation cover changes derived from a MMCO vegetation distribution produced by the dynamic vegetation model CARAIB, forced with the climate of the warmest and most humid experiment of the series. The boundary condition changes generally produce global warming in the Middle Miocene that are in agreement with previous Middle Miocene sensitivity experiments (Tong et al., 2009; You et al., 2009). However, the increases of temperature that we obtained are lower than those supported by proxy data (Zachos et al., 2001; Bruch et al., 2007).

The increase of the atmospheric CO₂ concentration to 500 ppmv produces the largest global warming of the series and contributes to warm the climate at all latitudes, in agreement with the results of previous modelling studies (Tong et al., 2009; You et al., 2009). Therefore, a higher than present-day CO₂ concentration seems necessary to produce the warm climate of the MMCO inferred from proxy-data. This result supports the terrestrial proxy reconstruction suggesting higher atmospheric CO₂ concentrations at the MMCO (Kürschner et al., 2008; Retallack, 2009), but it does not support the decoupling between CO₂ and temperature during the Middle Miocene suggested by the marine isotopic CO₂ reconstructions (Henderiks and Pagani, 2008; Pearson and Palmer, 2000).

Nevertheless, increasing only the CO₂ concentration is not sufficient to produce the required warming at the MMCO suggested by proxy-based reconstructions. The lowered topography and the changes in oceanic heat transfer and in ocean gateways configuration also produce significant regional effects that have to be taken into account. The topographic and oceanic forcings applied here have a lower impact on the global temperature than the CO₂ forcing, due to a number of regional effects that partially cancel each other on global average. However, they significantly affect the temperature and precipitation distributions and their local effects can exceed the CO₂ effect. The lower topography allows a more zonal atmospheric circulation and the westerly flow to continue over the lowered Plateaus at mid-latitudes. The reduced height of the Tibetan Plateau notably prevents the development of a monsoon-like circulation (Kutzbach et al., 1989; Harris, 2006). Our results also highlight the effect of the reduction of elevations of the North American and European reliefs, which strongly increases precipitation but decreases surface air temperature from northwestern to eastern Europe. The temperatures obtained over northern Europe are too cold relative to proxy-based temperature reconstruction of the European Middle Miocene climate (Mosbrugger et al., 2005), but the reduction of the seasonal gradient and the wetter conditions agree well with several proxy-based reconstructions (Jimenez-Moreno and Suc, 2007; Utescher et al., 2007; Mosbrugger et al., 2005).

Unfortunately, we were not able to take into account all the possible mechanisms that could contribute to the Middle Miocene warm climate. We notably could not take into account the complete ocean-atmosphere feedback loop that could be simulated with a fully coupled ocean-atmosphere model. We furthermore did not take into account a change in the concentrations of other atmospheric greenhouse gases such as methane.

The vegetation feedback also plays an important role in the warm MMCO climate, as demonstrated by the last experiment where we investigated the vegetation cover change feedback. In response to warm and humid conditions, forests expand at the expense of deserts and warm forest types develop poleward of the subtropical zone. Such a change in the vegetation cover leads to stronger warming and increase of precipitation. Moreover, the vegetation feedback on climate is of the same order of magnitude as the topographic or CO₂ effects, confirming the importance of the vegetation contribution to the MMCO climate. Therefore, vegetation-climate interactions could provide a complementary, if not an alternative mechanism, to the large increase of CO₂ required by the model to produce the estimated warming at the MMCO. This confirms the contribution of vegetation to the MMCO warm climate and emphasises the need for data-model comparison in order to estimate the reliability of climate model experiments and vegetation reconstructions.

Acknowledgements. We acknowledge the efforts of the Planet Simulator team (especially Klaus Fraedrich, Edilbert Kirk and Frank Lunkeit) for making available their model as Open Source Software and for the sustained development and help. We also thank the two anonymous reviewers for their constructive comments. A.-J. Henrot is a Research Fellow and G. Munhoven a Research Associate with the Belgian Fund for Scientific Research (F.R.S.-FNRS). We acknowledge support for this research from F.R.S.-FNRS under research grant “Crédit aux chercheurs” 1.5.179.07 F. This work is a contribution to the Deutsche Forschungsgemeinschaft project “Understanding Cenozoic Climate Cooling (UCCC)” (FOR 1070).

Edited by: M. Claussen

References

- Bice, K. L., Scotese, C. R., Seidov, D., and Barron, E. J.: Quantifying the role of geographic changes in Cenozoic ocean heat transport using uncoupled atmosphere and ocean models, *Earth Planet. Sci. Lett.*, 161, 295–310, 2000.
- Bruch, A. A., Uhl, D., and Mosbrugger, V.: Miocene climate in Europe. Patterns and evolution: a first synthesis of NECLIME, *Palaeogeogr., Palaeoclimatol., Palaeoecol.*, 253, 1–7, 2007.
- Butzin, M., Lohmann, G., and Bickert, T.: Miocene ocean circulation inferred from marine carbon cycle modeling combined with benthic isotope records, *Paleoceanography*, submitted, 2010.
- Currie, B. S., Rowley, D. B., and Tabor, N. J.: Middle Miocene paleoaltimetry of Southern Tibet: implications for the role of mantle thickening and delamination in the Himalayan orogen, *Geology*, 33, 181–184, 2005.
- Diester-Haass, L., Billups, K., Gröcke, D., François, L., Lefebvre, V., and Emeis, K.: Mid-Miocene paleoproductivity in the Atlantic Ocean and Implications for the Global Carbon Cycle, *Paleoceanography*, 24, PA1209, doi:10.1029/2008PA001605, 2009.
- Dutton, J. F. and Barron, E. J.: Miocene to present vegetation changes: A possible piece of the Cenozoic puzzle, *Geology*, 25, 39–41, 1997.
- Flower, B. P. and Kennett, J. P.: The Middle Miocene climatic transition: East Antarctic ice sheet development, deep ocean circulation and global carbon cycling, *Palaeogeogr., Palaeoclimatol., Palaeoecol.*, 108, 537–555, 1994.
- Forster, P., Ramaswamy, V., Artaxo, P., Bernsten, T., Betts, R., Fahey, D. W., Haywood, J., Lean, J., Lowe, D. C., Myhre, G., Nganga, J., Prinn, R., Raga, G., Schulz, M., and Van Dorland, R.: Changes in Atmospheric Constituents and in Radiative Forcing, in: *Climate Change 2007: The Physical Science Basis, Contribution of Working Group I to the Fourth Assessment Report of the Intergovernmental Panel on Climate Change*, edited by: Solomon, S., Qin, D., Manning, M., Chen, Z., Marquis, M., Averyt, K. B., Tignor, M., and Miller, H. L., Cambridge University Press, Cambridge, 2007.
- Fraedrich, K., Kirk, E., and Lunkeit, F.: PUMA Portable University Model of the Atmosphere, Tech. Rep. 16, Meteorologisches Institut, Universität Hamburg, Hamburg, 1998.
- Fraedrich, K., Jansen, H., Kirk, E., Luksch, U., and Lunkeit, F.: The Planet Simulator : Towards a user friendly model, *Meteorol. Z.*, 14, 299–304, doi:10.1127/0941-2948/2005/0043, 2005a.
- Fraedrich, K., Jansen, H., Kirk, E., and Lunkeit, F.: The Planet Simulator: Green planet and desert world, *Meteorol. Z.*, 14, 305–

- 314, doi:10.1127/0941-2948/2005/0044, 2005b.
- François, L., Ghislain, L., Otto, D., and Micheels, A.: Late Miocene vegetation reconstruction with the CARAIB model, *Palaeogeogr., Palaeoclimatol., Palaeoecol.*, 238, 302–320, 2006.
- Galy, V., François, L., France-Lanord, C., Faure, P., Kudrass, H., Palhol, F., and Singh, S. K.: C4 plants decline in the Himalayan basin since the Last Glacial Maximum, *Quat. Sci. Rev.*, 27, 1396–1409, 2008.
- Gladenkov, A., Oleinik, A. E., Marincovich, L. J., and Barinov, K. B.: A refined age for the earliest opening of the bering strait, *Palaeogeogr., Palaeoclimatol., Palaeoecol.*, 183, 321–328, 2002.
- Gregory-Wodzicki, K. M.: Uplift history of the Central and Northern Andes: A review, *Geol. Soc. Am. Bull.*, 112, 1091–1105, 2000.
- Grosfeld, K., Lohmann, G., Rimbu, N., Fraedrich, K., and Lunkeit, F.: Atmospheric multidecadal variations in the North Atlantic realm: proxy data, observations, and atmospheric circulation model studies, *Clim. Past*, 3, 39–50, 2007.
- Haberkorn, K., Sielmann, F., Lunkeit, F., Kirk, E., Schneidereit, A., and Fraedrich, K.: Planet Simulator Climate, Scientific report, Meteorological Institute, University of Hamburg, Hamburg, Germany, <http://www.mi.uni-hamburg.de/Downloads-un.245.0.html>, 2009.
- Harris, N.: The elevation history of the Tibetan Plateau and its implication for the Asian monsoon, *Palaeogeogr., Palaeoclimatol., Palaeoecol.*, 241, 4–15, 2006.
- Henderiks, J. and Pagani, M.: Coccolithophore cell size and the Paleogene decline in atmospheric CO₂, *Earth Planet. Sci. Lett.*, 269, 575–583, 2008.
- Henrot, A.-J.: Impacts des changements des propriétés de la surface terrestre sur le climat du dernier maximum glaciaire. Etude avec un modèle climatique, Master Thesis, University of Liège, Liège, Belgium, 2007.
- Henrot, A.-J., François, L., Brewer, S., and Munhoven, G.: Impacts of land surface properties and atmospheric CO₂ on the Last Glacial Maximum climate: a factor separation analysis, *Clim. Past*, 5, 183–202, 2009.
- Herold, N., Seton, M., Müller, R. D., You, Y., and Huber, M.: Middle Miocene tectonic boundary conditions for use in climate models, *Geochem., Geophys., Geosyst.*, 9(10), Q10009, doi:10.1029/2008GC002046, 2008.
- Herold, N., You, Y., Müller, R. D., and Seton, M.: Climate model sensitivity to change in Miocene paleotopography, *Austral. J. Earth Sci.*, 56, 1049–1059, 2009.
- Jimenez-Moreno, G. and Suc, J.-P.: Middle Miocene latitudinal climatic gradient in Western Europe: Evidence from pollen records, *Palaeogeogr., Palaeoclimatol., Palaeoecol.*, 253, 208–225, 2007.
- Junge, M. M., Lunkeit, F., Fraedrich, K., Gayler, V., Blender, R., and Luksch, U.: A world without Greenland: impacts on Northern Hemisphere circulation in low and high resolution models, *Climate Dyn.*, 24, 297–307, 2005.
- Kuhlemann, J., Dunkl, I., Brügel, A., Spiegel, C., and Frisch, W.: From source terrains of the Eastern Alps to the Molasse Basin: Detrital record of non-steady-state exhumation, *Tectonophysics*, 413, 301–316, 2006.
- Kürschner, W. M., Kvacek, Z., and Dilcher, D. L.: The impact of Miocene atmospheric carbon dioxide fluctuations on climate and the evolution of terrestrial ecosystems, *PNAS*, 105, 449–453, 2008.
- Kutzbach, J. E., Ruddiman, W. F., and Prell, W. L.: Sensitivity of Climate to late Cenozoic Uplift in Southern Asia and the American West: Numerical Experiments, *J. Geophys. Res.*, 94, 393–407, 1989.
- Laurent, J.-M., François, L., Bar-Hen, A., Bel, L., and Cheddadi, R.: European Bioclimatic Affinity Groups: data-model comparisons, *Global Planet. Change*, 61, 28–40, 2008.
- Lunt, D. J., Valdes, P. J., Haywood, A., and Rutt, I. C.: Closure of the Panama Seaway during the Pliocene: implications for climate and Northern Hemisphere glaciation, *Climate Dyn.*, 30, 1–18, 2008.
- Maier-Reimer, E., Mikolajewicz, U., and Hasselmann, K.: Mean Circulation of the Hamburg LSG OGCM and Its Sensitivity to the Thermohaline Surface Forcing, *J. Phys. Oceanogr.*, 23, 731–757, 1993.
- Micheels, A., Bruch, A., and Mosbrugger, V.: Miocene climate modelling sensitivity experiments for different CO₂ concentrations, *Palaeontologia Electronica*, 12, 2009a.
- Micheels, A., Eronen, J., and Mosbrugger, V.: The Late Miocene climate response to a modern Sahara desert, *Global Planet. Change*, 67, 193–204, 2009b.
- Mosbrugger, V., Utescher, T., and Dilcher, D. L.: Cenozoic continental climatic evolution of Central Europe, *Proc. Nat. Acad. Sci.*, 102, 14964–14969, 2005.
- Myhre, G., Highwood, E. J., Shine, K. P., and Stordal, F.: New estimates of radiative forcing due to well mixed greenhouse gases, *Geophys. Res. Lett.*, 25(14), 2715–2718, 1998.
- New, M., Lister, D., Hulme, M., and Makin, I.: A high-resolution data set of surface climate over global land areas, *Clim. Res.*, 21, 1–25, 2002.
- Okumura, Y. M., Deser, C., Hu, A., Timmermann, A., and Xie, S.-P.: North Pacific Climate Response to Freshwater Forcing in the Subarctic North Atlantic: Oceanic and Atmospheric Pathways, *J. Climate*, 22, 1424–1445, 2009.
- Otto, D., Rasse, D., Kaplan, J., Warnant, P., and François, L.: Biospheric carbon stocks reconstructed at the Last Glacial Maximum: comparison between general circulation models using prescribed and computed sea surface temperatures, *Global Planet. Change*, 33, 117–138, 2002.
- Pagani, M., Arthur, M. A., and Freeman, K. H.: Miocene evolution of atmospheric carbon dioxide, *Paleoceanography*, 14, 273–292, 1999.
- Pagani, M., Zhonghui, L., LaRiviere, J., and Ravelo, A. C.: High Earth-system climate sensitivity determined from Pliocene carbon dioxide concentrations, *Nat. Geosci.*, 3, 27–30, 2010.
- Pearson, P. N. and Palmer, M. R.: Atmospheric carbon dioxide concentrations over the past 60 million years, *Nature*, 406, 695–699, 2000.
- Pearson, P. N., van Dongen, B. E., Nicholas, C. J., Pancost, R. D., Schouten, S., Singano, J. M., and Wade, B. S.: Stable warm tropical climate through the Eocene Epoch, *Geology*, 35, 211–214, 2007.
- Pekar, S. F. and DeConto, R. M.: High-resolution ice-volume estimates for the early Miocene: Evidence for a dynamic ice sheet in Antarctica, *Palaeogeogr., Palaeoclimatol., Palaeoecol.*, 231, 101–109, 2006.
- Peltier, W. R.: Global glacial isostasy and the surface of the ice-age Earth: the ICE-5G (VM2) Model and GRACE, *Annu. Rev. Earth Planet. Sci.*, 32, 49–111, 2004.

- Retallack, G. J.: Refining a pedogenic-carbonate CO₂ paleobarometer to quantify a middle Miocene greenhouse spike, *Palaeogeogr., Palaeoclimatol., Palaeoecol.*, 281, 57–65, 2009.
- Romanova, V., Lohmann, G., and Grosfeld, K.: Effect of land albedo, CO₂, orography, and oceanic heat transport on extreme climates, *Clim. Past*, 2, 31–42, 2006.
- Ruddiman, W. F.: *Tectonic Uplift and Climate Change*, Plenum Press, New York, NY, 1997.
- Schneider, B. and Schmittner, A.: Simulating the impact of the Panamanian seaway closure on ocean circulation, marine productivity and nutrient cycling, *Earth Planet. Sci. Lett.*, 246, 367–380, 2006.
- Shellito, C. J., Sloan, L. C., and Huber, M.: Climate model sensitivity to atmospheric CO₂ levels in the Early-Middle Paleogene, *Palaeogeogr., Palaeoclimatol., Palaeoecol.*, 193, 113–123, 2003.
- Tong, J. A., You, Y., Müller, R. D., and Seton, M.: Climate model sensitivity to atmospheric CO₂ concentrations for the middle Miocene, *Global Planet. Change*, 67, 129–140, 2009.
- Tschuck, P., Chauvin, F., Dong, B., and Arpe, K.: Impact of sea-surface temperature anomalies in the Equatorial Indian Ocean and Western Pacific on the Asian summer monsoon in three general circulation models, *Int. J. Climatol.*, 24, 181–191, 2004.
- Utescher, T., Mosbrugger, V., and Ashraf, A.: Terrestrial climate evolution in Northwest Germany over the last 25 million years, *Palaeogeogr., Palaeoclimatol., Palaeoecol.*, 15, 430–449, 2000.
- Utescher, T., Erdei, B., François, L., and Mosbrugger, V.: Tree diversity in the Miocene forests of Western Eurasia, *Palaeogeogr., Palaeoclimatol., Palaeoecol.*, 253, 226–250, 2007.
- Van Dam, J. A.: Geographic and temporal patterns in the late Neogene (12–3 Ma) aridification of Europe. The use of small mammals as paleoprecipitation proxies, *Palaeogeogr., Palaeoclimatol., Palaeoecol.*, 238, 190–218, 2006.
- Von der Heydt, A. and Dijkstra, H. A.: Effect of ocean gateways on the global ocean circulation in the late Oligocene and early Miocene, *Paleoceanography*, 21, PA1011, 2006.
- Von der Heydt, A. and Dijkstra, H. A.: The effect of ocean gateways on ocean circulation patterns in the Cenozoic, *Global Planet. Change*, 62, 132–146, 2008.
- Wang, Y., Deng, T., and Biasatti, D.: Ancient diets indicate significant uplift of southern Tibet after ca. 7 Ma, *Geology*, 34, 309–312, 2006.
- Williams, M., Haywood, A. M., Taylor, S. P., Valdes, P. J., Sellwood, B. W., and Hillenbrand, C. D.: Evaluating the efficacy of planktonic foraminifer calcite $\delta^{18}\text{O}$ data for sea surface temperature reconstruction for the Late Miocene, *Geobios*, 38(6), 843–863, 2005.
- You, Y., Huber, M., Müller, R. D., Poulsen, C. J., and Ribbe, J.: Simulation of the Middle Miocene Climate Optimum, *Geophys. Res. Lett.*, 36, L04702, doi:10.1029/2008GL036571, 2009.
- Zachos, J., Pagani, M., Sloan, L., Thomas, E., and Billups, K.: Trends, rhythms and aberrations in global climate 65 Ma to present, *Science*, 292, 686–693, 2001.